DESY T-95-02

The Electroweak Phase Transition

DISSERTATION

zur Erlangung des Doktorgrades
des Fachbereichs Physik
der Universität Hamburg

vorgelegt von
ARTHUR HEBECKER
aus Moskau

Hamburg
1995

Gutachter der Dissertation:	Prof. Dr. W. Buchmüller Prof. Dr. G. Mack Prof. Dr. C. Wetterich
Gutachter der Disputation:	Prof. Dr. W. Buchmüller Prof. Dr. J. Bartels
Datum der Disputation:	2. Mai 1995
Sprecher des Fachbereichs Physik und Vorsitzender des Promotionsausschusses:	Prof. Dr. B. Kramer

Abstract

The electroweak phase transition is investigated by means of the perturbatively calculated high temperature effective potential. An analytic result to order g^4, λ^2 is presented for the Abelian Higgs model, the SU(2)-Higgs model and the standard model and a complete on-shell renormalization at zero temperature is performed. Higher order corrections are found to increase the strength of the first order phase transition in the non-Abelian model, opposite to the Abelian case. This effect is traced back to the infrared contributions from the typical non-Abelian diagrams. The dependence of several phase transition parameters on the Higgs mass is analysed in detail. A new, gauge invariant, approach based on the composite field $\Phi^\dagger\Phi$ is introduced. This method, which supports the above Landau gauge results numerically, permits a conceptually simpler treatment of the thermodynamics of the phase transition. In particular, it enables a straightforward comparison with lattice data and the application of the Clausius-Clapeyron equation to the electroweak phase transition.

Zusammenfassung

Der elektroschwache Phasenübergang wird mit Hilfe des störungstheoretisch berechneten effektiven Potentials der Hochtemperaturfeldtheorie untersucht. Für das abelsche Higgs-Modell, das SU(2)-Higgs-Modell und das Standardmodell werden analytische Ergebnisse der Ordnung g^4, λ^2 angegeben, und eine vollständige Renormierung im On-Shell-Schema bei Temperatur Null wird durchgeführt. Im Gegensatz zum abelschen Fall führen die Korrekturen höherer Ordnung beim nichtabelschen Modell zu einer Verstärkung des Phasenüberganges erster Ordnung. Dieser Effekt wird auf die infraroten Beiträge typischer nichtabelscher Diagramme zurückgeführt. Die Abhängigkeit mehrerer Parameter des Phasenüberganges von der Higgs-Masse wird einer detaillierten Analyse unterzogen. Ein neuer, eichinvarianter Zugang, der sich auf das zusammengesetzte Feld $\Phi^\dagger\Phi$ stützt, wird eingeführt. Diese Methode bestätigt numerisch die obigen, in Landau-Eichung erzielten Resultate und erlaubt eine begrifflich einfachere Behandlung der Thermodynamik des Phasenüberganges. Insbesondere ermöglicht sie den unmittelbaren Vergleich mit Gitter-Daten und die Anwendung der Clausius-Clapeyron-Gleichung auf den elektroschwachen Phasenübergang.

Contents

Introduction

The whole known universe consists almost exclusively of matter, with no considerable amount of antimatter in our galaxy cluster and no known mechanism to separate matter and antimatter on such large scales [1]. This baryon asymmetry of the universe is one of the most interesting cosmological problems to be resolved by particle theory.

As pointed out by Sakharov in 1967 the baryon asymmetry may be a calculable result of particle interactions [2], the necessary conditions being baryon number violation, C– and CP–violation, and departure from thermal equilibrium.

Kirzhnits and Linde realized in 1972 that at high temperatures the spontaneously broken electroweak symmetry is restored, thus suggesting a phase transition in the early universe [3]. Since anomalous baryon number violation in the standard model is rapid at high temperatures, the departure from equilibrium in a first order electroweak phase transition opens the possibility of standard model baryogenesis. This scenario, first suggested by Kuzmin, Rubakov and Shaposhnikov in 1985 [4], provides the main motivation for the present investigation. Although more recent analyses seem to discourage baryogenesis within the minimal standard model due to the small CP-violation, simple non-minimal models may produce a sufficient asymmetry (see [5] and references therein). In any case it is clear that the present baryon asymmetry of the universe has been finally determined at the electroweak phase transition, since baryon-number violating processes fall out of thermal equilibrium at the corresponding critical temperature.

A quantitative understanding of the electroweak phase transition is a basic prerequisite for the discussion of any model of baryogenesis at the weak scale. This includes reliable knowledge of its order and of the strength of the phase transition, if it is of first order. Several approaches have been used to investigate the electroweak phase transition. Important results have been obtained by use of 3-dimensional effective theory [6, 7], ϵ-expansion [8], average action [9] and lattice simulations [10–12]. In particular, the detailed lattice data for physical phase transition parameters from refs. [11, 12] permit explicit comparison with results from

perturbation theory.

The present investigation is concerned with the extraction of thermodynamic parameters of the electroweak phase transition, based on the perturbative calculation of the high temperature effective potential, i.e. the free energy of the system.

Perturbative calculations of the potential to the order $g^3, \lambda^{3/2}$ suggest a first order phase transition for different Higgs models (g denotes the gauge coupling and λ the scalar coupling). These calculations, based on the one-loop ring summation, have been carried out in refs. [13, 14] for the Abelian Higgs model and in refs. [15, 16] for the standard model. Two-loop summation has been done to order g^4, λ in ref. [17], where scalar masses have been neglected with respect to gauge boson masses, and by use of another approximation in ref. [18]. The results of ref. [17] include both the Abelian and the non-Abelian case.

However, there is a need to extend the work of Arnold and Espinosa [17] to a complete g^4, λ^2-calculation. In the present investigation, assuming formally $\lambda \sim g^2$ and keeping the full dependence on the Higgs field φ, its zero temperature vacuum expectation value v and the temperature T, the necessary corrections are calculated [19, 20]. To obtain information about the importance of specific non-Abelian effects and to have a particularly simple model, the Abelian case has been considered first [19].

Besides the above extension of a conventional approach, a gauge invariant calculation of phase transition parameters is presented [21, 22]. Using this method a better understanding of the physics of the phase transition is obtained. The numerical results of the gauge invariant approach are similar to conventional Landau gauge calculations, thus supporting their reliability.

Chapter 1 starts with some well known facts about the effective potential, its thermodynamic interpretation, its loop expansion and the relevance for the description of first order phase transitions. After that the resummation of masses, necessary at high temperature, is discussed. Here the emphasis is on a method based on Dyson-Schwinger equations [19, 20] to be used in the sequel.

In chapter 2 the complete g^4, λ^2 calculation of the finite temperature effective potential is performed for the Abelian Higgs model [19]. This includes a zero temperature renormalization in the on-shell scheme. The absence of a linear φ-term, explicitly verified at this order, is shown to survive to all orders. Latent heat, surface tension and jump of the order parameter are calculated as functions of the Higgs mass from different approximations to the effective potential. The higher order scalar corrections, added to the previous results,

are found to be important at not too small Higgs masses.

The above analysis is extended to the standard model in chapter 3 which is based on ref. [20]. First, the case of the pure SU(2)-Higgs model, which is much simpler, is discussed in detail. The importance of specifically non-Abelian contributions is stressed and the uncertainties of perturbation theory are traced back to infrared problems. A qualitatively similar situation is found for the complete standard model. The main quantitative change is introduced by the large top mass, which reduces the strength of the first order phase transition.

In the last chapter the gauge invariant approach to the phase transition, suggested in ref. [21], is described. The phase transition parameters obtained from a one-loop calculation are compared with the Landau gauge results, showing good agreement for not too large Higgs masses. Several additional questions of the analysis of the electroweak phase transition are discussed in the sequel [22]. They include two-loop resummation problems, the connection of gauge invariant and Landau gauge approach, and the use of the Clausius-Clapeyron equation in the present context.

After the discussion of conclusions to be drawn from the above investigation several analytic formulae are listed in the appendices. Appendix A contains some useful integrals. The explicit analytic results for the finite temperature effective potential in the Abelian Higgs model, the SU(2)-Higgs model and the standard model are displayed in appendix B. Self energy corrections at zero temperature, necessary for the on-shell renormalization, are given in appendix C.

Chapter 1

The effective potential

1.1 Definition and loop expansion

The present investigation is concerned with equilibrium thermodynamics, which, as is well known, can be completely described as soon as the partition function

$$Z = \mathbf{tr} \exp\left[-\beta(\boldsymbol{H} + \int_V J\varphi)\right] \tag{1.1}$$

of the system under consideration is given. Here the inverse temperature is denoted by β and $\boldsymbol{H}$ is the Hamilton operator. The source J is coupled to the field φ, specified later on as the Higgs field, which is used as the order parameter for the description of the phase transition. In this section it is sufficient to consider the simplest possible case of a φ^4-model with one degree of freedom. The generalization to more complicated field theories is straightforward.

The fundamental thermodynamic potential per unit volume, $W(J)$, is related to the partition function by

$$Z = \exp(-\beta\Omega W)\,, \tag{1.2}$$

where Ω denotes the three dimensional volume of the physical system. The temperature dependent effective potential is now defined by the transition from the variable J to the variable φ, realized by a Legendre transformation:

$$V(\varphi,T) = W(J,T) - J\varphi \qquad , \qquad \varphi = \frac{\partial W(J,T)}{\partial J}. \tag{1.3}$$

It is straightforward to derive the two identities

$$< \varphi >= \varphi = \frac{\partial W}{\partial J} \qquad , \qquad \frac{1}{\Omega} < \boldsymbol{H} > \Big|_{< \varphi >= \varphi} - TS = V(\varphi,T) \tag{1.4}$$

clarifying the physical interpretation of the effective potential as the free energy of the system. Here the brackets $< ... >$ symbolize the thermal expectation value of an operator and $S = -\partial W/\partial T$ is the entropy.

The perturbative calculation developed later on is based on the path integral representation of the partition function [23]

$$Z = \mathbf{tr} \exp\left[-\beta(\boldsymbol{H} + \int_V J\varphi)\right] = \int D\varphi_{\text{period.}} \exp\left[\int_0^\beta d\tau \int d^3\vec{x}(\mathcal{L} - J\varphi)\right] . \tag{1.5}$$

Here $\mathcal{L}$ is the Euclidean Lagrangian and the path integral is taken over all fields periodic in time direction. Compactification of Euclidean time results in the replacement of the well known loop integral by the integral-sum

$$\sum\!\!\!\!\!\!\int dk = \frac{T}{(2\pi)^3} \sum_{n=-\infty}^{n=+\infty} \int d^3\vec{k} \tag{1.6}$$

and correspondingly in the introduction of the Euclidean propagator with discrete Matsubara frequencies k_0

$$\frac{1}{k^2 + m^2} = \frac{1}{k_0^2 + \vec{k}^2 + m^2} \qquad , \qquad k_0 = 2\pi T n. \tag{1.7}$$

This imaginary time formalism, used exclusively in the following, is the simplest formulation of finite temperature field theory and perfectly suited for the investigation of the desired equilibrium parameters.

While Z is the sum of all Feynman diagrams, $\beta\Omega W = -\ln Z$ contains the connected graphs only. The potential V, obtained from W by means of a Legendre transformation, is the momentum independent part of the generating functional of one-particle irreducible diagrams. It has to be evaluated at non-vanishing external field, thus requiring the summation of infinitely many graphs at each loop order. This problem is solved by the following identity [24]:

$$V(\hat{\varphi}) = V_{tree}(\hat{\varphi}) + \frac{1}{2} \sum\!\!\!\!\!\!\int dk \ln(k^2 + m_{\hat{\varphi}}^2) + \Big\{\text{one-particle irred. vacuum diagrams}\Big\}. \tag{1.8}$$

Here V_{tree} denotes the tree-level potential, i.e. the momentum independent part of the free Hamiltonian. The curly bracket represents the sum of all one-particle irreducible vacuum graphs calculated from the 'shifted' Lagrangian

$$\mathcal{L}^{\hat{\varphi}}(\varphi) = \mathcal{L}(\hat{\varphi} + \varphi) - \Big\{\text{terms, constant and linear in } \varphi\Big\} . \tag{1.9}$$

Correspondingly, $m_{\hat{\varphi}}^2$ is the mass term generated after this shift.

The perturbative methods described in section 1.3 are based on the above representation of the potential. Note that in the following sections, the shift $\hat{\varphi}$ will often be denoted by φ for brevity, if no confusion is possible.

In the remainder of this section a short derivation of the identity (1.8) shall be given. To keep the notation compact, let $\beta = \Omega = 1$ during these manipulations.

Shifting the integration variable in eq. (1.5) by some arbitrary but fixed function $\tilde{\varphi}$ results in

$$W[J] = -\ln \int D\varphi \exp\left[\int \mathcal{L}(\varphi+\tilde{\varphi}) - (\varphi+\tilde{\varphi})J\right], \tag{1.10}$$

where the Lagrangian after the shift can be written in the form

$$\mathcal{L}(\varphi+\tilde{\varphi}) = -V_{tree}(\tilde{\varphi}) - \varphi g(\tilde{\varphi}) + \mathcal{L}^{\tilde{\varphi}}(\varphi)\,. \tag{1.11}$$

Note that J is not necessarily constant and W is a functional. The effective action is defined by

$$\Gamma[\hat{\varphi}] = -W[J] + \int J\hat{\varphi} \qquad , \qquad \hat{\varphi} = \frac{\delta W}{\delta J}\,, \tag{1.12}$$

where arguments have been dropped for brevity in the functional derivative. Introducing the notation $\tilde{J} = J + g(\tilde{\varphi})$ and using the generating functional of the 'shifted' theory

$$W^{\tilde{\varphi}}[J] = -\ln \int D\varphi \exp\left[\int \mathcal{L}^{\tilde{\varphi}}(\varphi) - \varphi J\right], \tag{1.13}$$

the effective action takes the form

$$\Gamma[\hat{\varphi}] = -V_{tree}(\tilde{\varphi}) - W^{\tilde{\varphi}}[\tilde{J}] + \int(\hat{\varphi}-\tilde{\varphi})J\,. \tag{1.14}$$

Observe that

$$\hat{\varphi} = \frac{\delta W[J]}{\delta J} = \frac{\delta W[J]}{\delta \tilde{J}} = \tilde{\varphi} + \frac{\delta W^{\tilde{\varphi}}[\tilde{J}]}{\delta \tilde{J}}\,. \tag{1.15}$$

Now the shift $\tilde{\varphi}$, which has not yet been specified, is set to $\tilde{\varphi} = \hat{\varphi}$. This gives an explicit result for the effective action:

$$\Gamma[\hat{\varphi}] = -V_{tree}(\hat{\varphi}) - W^{\hat{\varphi}}[\tilde{J}] \quad \text{at} \quad \frac{\delta W^{\hat{\varphi}}}{\delta \tilde{J}} = 0\,. \tag{1.16}$$

Since the effective potential is given by minus the momentum independent part of Γ, the identity (1.8) follows.

1.2 Description of a first order phase transition

The intuitive picture of a first order phase transition, described by the free energy density of the system, is based on the double well structure of the free energy as a function of the order parameter. In this picture the barrier between the two minima is responsible for the

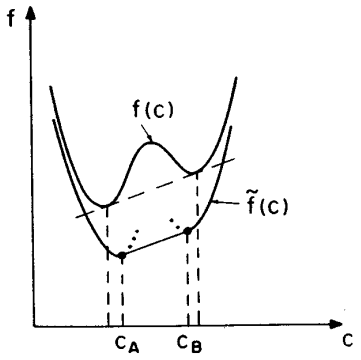

Fig.1.1 Schematic graph of the coarse-grained free energy, $f(c)$, and the corresponding true free energy, $\tilde{f}(c)$. The dotted sections denote the analytic continuation of $\tilde{f}(c)$ into the metastable region (from Langer, [25])

necessity of an activation energy for a transition between the phases, thus rendering the phase transition first order. However, a rigorous definition of such a non-convex free energy is not trivial. First the phenomenological discussion of Langer [25] shall be briefly described:

Assume the existence of a coarse-grained free energy, $F(c)$, of the form

$$F(c) = \int_V \left[\frac{1}{2}(\partial c)^2 + f(c)\right] , \tag{1.17}$$

with some function $f(c)$ characterizing the homogeneous state and an order parameter c of the system. The free energy density f, typically of the form given in fig. 1.1, is well suited for the description of the metastable and unstable region. However, even in the region where f has a positive second derivative it is not identical with the true free energy density $\tilde{f}$. The later one is a convex function and connects the two different physical states of the system by a straight line. In the metastable, though not in the unstable region, the analytic continuation of $\tilde{f}(c)$ does still describe the thermodynamic properties of the one-phase physical system.

The perturbatively calculated high temperature effective potential is by definition an analytic function of the order parameter φ. Therefore, assuming its convergence to the true free energy in the stable region [26,27], it can be naturally interpreted in the above sense as the free energy of the metastable states. This, however, does not clarify the interpretation in the unstable, non-convex region of the potential.

Following Langer, the coarse-grained free energy can be calculated by integrating out the short wavelength components of the microscopic variable only. This corresponds to the introduction of some infrared cutoff characterizing the coarse-graining size. Note that the one-loop results for the effective potential are not very sensitive to a small enough infrared cutoff. In fact, in the Abelian model no infrared problems are expected at any loop-order (see section 2.3). Even the non-Abelian two-loop results of section 3.3.1 do not change qualitatively when a small infrared cutoff is introduced. This could be taken as a justification to interpret the non-convex region of the obtained effective potential in the spirit

of the coarse-grained free energy. A detailed discussion of the coarse-grained free energy in high temperature field theory can be found in ref. [28].

At one-loop level such an interpretation is supported by the analysis of ref. [29]. There it is shown that in some approximation the effective potential $V(\varphi)$ gives the energy density of a homogeneous state with wave functional concentrated on configurations near the classical value φ.

It has to be admitted that the understanding of the perturbatively calculated effective potential in the non-convex region does not seem to be satisfactory. This implies some doubts about the physical interpretation of quantities calculated from the potential in that region. In particular, the surface tension, as it is defined and calculated in chapters 2 and 3 is affected by this uncertainty.

Nevertheless, critical temperature, latent heat and jump of the order parameter are, in principle, calculable by standard methods from the effective potential. This is due to the fact that they can be obtained from the minima of the free energy, which, following the above discussion, are trustworthily described by the potential.

1.3 Resummation

The loop expansion of the potential given by eq. (1.8) formally corresponds to an expansion in coupling constants. Unfortunately, due to the effectively three dimensional integrals arising from contributions with vanishing Matsubara frequencies in the high temperature theory terms proportional to $(T/m)^n$ do appear. Owing to the Higgs mechanism masses are proportional to coupling constants in the relevant theories. Therefore a formal loop expansion does not generate the desired expansion in coupling constants. This problem is well known and can be solved by resummation. In the following this shall be described in detail for some unspecified theory with a generic coupling constant g, to be used as the expansion parameter:

Consider a general Lagrangian with interaction terms generating 3- and 4-vertices proportional to g^2 and 3-vertices proportional to $g\,k_\mu$. Here k_μ is a momentum variable, as it appears at the vertex in gauge theories. All masses are considered to be of order g. Note that this structure is suggested by the standard model Lagrangian, where the square root of the scalar coupling $\sqrt{\lambda}$, the Yukawa coupling g_Y, the electroweak gauge couplings g_1, g_2 and the strong gauge coupling g_s play the role of the generic coupling g. The Abelian Higgs model and the SU(2)-Higgs model fit this general structure as well [14,16,30].

Resummation now means that the leading self-energy corrections of order g^2T^2 have to be added to the mass squares, thereby collecting an infinite series of graphs with increasing powers of (gT/m). Having realized that in a systematic way, the remaining higher loop corrections are always connected with higher orders in the couplings, which ensures a systematic expansion of the potential [16].

Working in that spirit, the main task is now to identify all graphs contributing to the order g^4.

1.3.1 Method based on Dyson-Schwinger equations

In this subsection a method for the calculation of the effective potential based on Dyson-Schwinger equations is presented [19, 20]. A similar way of summing the different contributions to V for the φ^4-theory has been considered in ref. [31].

To circumvent the combinatoric problems of resummation it is useful not to calculate the potential $V(\varphi)$ itself but its derivative with respect to the field φ, i.e. the sum of all one-particle irreducible one-point functions. This 'tadpole' method has been suggested in refs. [32].

The Dyson-Schwinger equation [33] for the effective potential has the form

$$-\frac{\partial}{\partial\varphi}(V - V_{tree}) = A + B =$$

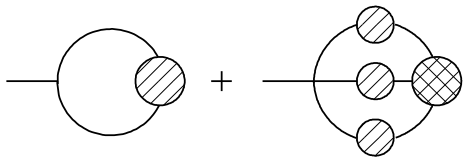

, (1.18)

where the internal lines represent all particles of the relevant theory and the external lines stand for the shifted scalar field. The two different sorts of blobs are full propagator and full 3-vertex respectively. Therefore the first term has the explicit form

$$A = \mathrm{tr}\,\mathcal{W}(\varphi)\sum\!\!\!\!\!\!\int \frac{dk}{k^2 + m_{tree}^2 + \Pi(k)}\,. \tag{1.19}$$

In general, mass, self-energy and vertex $\mathcal{W}$ are matrices and "tr" denotes the sum over the suppressed indices. The φ-dependence of the mass m_{tree}, introduced by the shift (1.9), is obvious.

No corrections are needed for the vertex function in the second term of eq. (1.18). This can be verified by the following argument: Any correction to that vertex corresponds to a proper three-loop contribution to the potential. Here by *proper*, the absence of self-energy insertions, which would require resummation, is meant. The three-dimensional contribution

to the three-loop graph, arising when all Matsubara frequencies vanish, results in a g^5-correction. This can be seen most easily by scaling all loop momenta according to $\vec{k} \to \vec{k}g$. Similar arguments do also prove that the parts of three-loop diagrams with non-vanishing Matsubara frequencies do not contribute φ-dependent terms to the potential up to order g^4. This way of argumentation is explained in more detail in ref. [30]. Appendix A of ref. [16] contains a proof of the sufficiency of self-energy resummation for the order g^3-potential, which can be generalized to higher orders.

The self-energy insertions needed in both terms of eq. (1.18) can again be obtained from a Dyson-Schwinger equation, which, to the required leading order, reads

$$-\Pi(k) = -(\Pi_a(k) + \Pi_b(k)) = \quad + \quad . \tag{1.20}$$

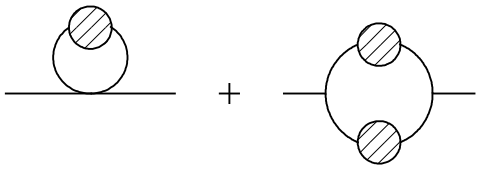

It is easily verified that the omitted parts would result in proper three-loop terms in the potential which do not contribute to the order g^4. In the following the indices 2 and 3 denote contributions of order g^2 and g^3 respectively. The tadpole part of the self-energy can be written as

$$\Pi_a(k) = \Pi_{a2} + \Pi_{a2}(k) + \Pi_{a3} + \cdots \quad , \quad \text{with} \quad \Pi_{a2}(0) = 0\,. \tag{1.21}$$

Here the momentum dependent part $\Pi_{a2}(k)$ does only arise in the case of a non-Abelian gauge theory. It is introduced by the corresponding projection operator when calculating the longitudinal self-energy of the gauge boson (see section 3.1).

The third order term in g does not contribute in the case of nonzero k_0. If $k_0 = 0$, by the above scaling argument $\vec{k} \to \vec{k}g$ only its momentum independent part Π_{a3} is needed.

The leading order momentum independent g^2-part of $\Pi_b(k)$ will be called Π_{b2}. All these contributions to the self-energy $\Pi(k)$, needed below, are obtained by iterating eq. (1.20) twice.

Using these definitions and introducing the corrected mass term m^2,

$$m^2 = m^2_{tree} + \Pi_{a2} + \Pi_{b2} \quad , \tag{1.22}$$

equation (1.19) can be written as

$$A = \operatorname{tr} \mathcal{W}(\varphi) \sum\!\!\!\!\!\!\int \frac{dk}{k^2 + m^2 + \Pi_{a2}(k) + \Pi_{a3} + \Pi_b(k) - \Pi_{b2}}$$

$$= \mathrm{tr}\,\mathcal{W}(\varphi)\sum\!\!\!\!\!\!\int dk \left(\frac{1}{k^2+m^2+\Pi_{a2}(k)} - \frac{1}{k^2+m^2}\Pi_{a3}\frac{1}{k^2+m^2} \right.$$
$$\left. + \frac{1}{k^2+m^2}\Pi_{b2}\frac{1}{k^2+m^2} - \frac{1}{k^2+m^2}\Pi_b(k)\frac{1}{k^2+m^2} \right). \qquad (1.23)$$

Here the second equality is obtained by expanding the integrand in g. Separate treatment of the parts with $k_0 = 0$ and $k_0 \neq 0$ together with the above scaling argument show that all contributions of order g^4 are taken into account.

Inspection of the last term of eq. (1.23) and term B of eq. (1.18) shows that their sum is equal to the derivative $-\partial V_\ominus/\partial\varphi$, where $-V_\ominus$ represents the sum of all two-loop diagrams of the type shown in fig. 1.2.a (setting sun diagrams). To see this, notice that

$$\mathcal{W}(\varphi) = -\frac{1}{2}\frac{\partial}{\partial\varphi}m^2\,, \qquad (1.24)$$

a direct consequence of the shift generating both mass terms and 3-vertices from the interaction Lagrangian. This observation simplifies the actual calculation significantly.

Furthermore, the contribution

$$V_z = \int^\varphi d\varphi' \mathrm{tr}\,\mathcal{W}(\varphi')\sum\!\!\!\!\!\!\int dk \frac{1}{k^2+m^2}\Pi_{a3}\frac{1}{k^2+m^2} \qquad (1.25)$$

is treated separately. It is equal to the sum of all terms bilinear in masses coming from two-loop diagrams of the type shown in fig. 1.2.b, i.e. the sum of their three-dimensional parts. Note that here and in the setting sun diagrams discussed above, masses resummed to leading order have to be used.

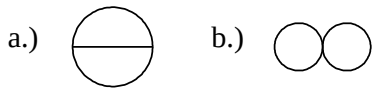

Fig.1.2 Typical two-loop diagrams

The remaining part

$$V_R = -\int^\varphi d\varphi'\,\mathrm{tr}\,\mathcal{W}(\varphi')\sum\!\!\!\!\!\!\int dk \left(\frac{1}{k^2+m^2+\Pi_{a2}(k)} + \frac{1}{k^2+m^2}\Pi_{b2}\frac{1}{k^2+m^2} \right) \qquad (1.26)$$

can be easily rewritten as

$$V_R = \frac{1}{2}\int dm^2\,\mathrm{tr}\sum\!\!\!\!\!\!\int \frac{dk}{k^2+m^2} + \frac{1}{2}\,\mathrm{tr}\sum\!\!\!\!\!\!\int \frac{dk}{k^2+m^2}(\Pi_{a2}(k)-\Pi_{b2})\,. \qquad (1.27)$$

Therefore the complete potential is given by

$$V = V_{tree} + V_\ominus + V_z + V_R\,. \qquad (1.28)$$

Denoting by V_3 the sum of the tree level potential and the g^3-order part of V_R and calling V_4 the fourth order corrections of V_R,

$$V_3 + V_4 = V_{tree} + V_R, \tag{1.29}$$

the following final formula is obtained :

$$V = V_3 + V_4 + V_\ominus + V_z. \tag{1.30}$$

This representation, used for the explicit results in the appendix, has the advantage of a separation of the third order part from the higher order corrections.

1.3.2 Counterterm method

Another possibility of a systematic resummation at high temperature is based on the introduction of thermal counterterms [34]. The simplest form of this method is to add and subtract a temperature dependent mass term for every field in the Lagrangian. Let

$$\mathcal{L} = \mathcal{L}_{kin} + \mathcal{L}_{mass} + \mathcal{L}_I \quad \text{with} \quad \mathcal{L}_{mass} = -\sum_i \frac{1}{2} m_{0i}^2 \varphi_i^2 \tag{1.31}$$

be the Euclidean Lagrangian depending on several fields φ_i, with kinetic term, mass term and interaction term. The leading temperature dependent mass corrections are given by

$-\delta m_i^2 = -\Pi_{2i}(0) =$ 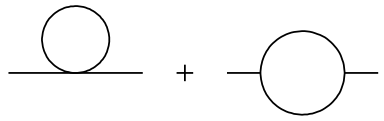 , (1.32)

where only the g^2T^2-pieces of the diagrams are considered. The Lagrangian is now rewritten according to

$$\begin{gathered} \mathcal{L} = \mathcal{L}_{kin} + \mathcal{L}'_{mass} + \mathcal{L}'_I \,, \\ \mathcal{L}'_{mass} = -\sum_i \frac{1}{2}(m_{0i}^2 + \delta m_i^2)\varphi_i^2 \qquad , \qquad \mathcal{L}'_I = \mathcal{L}_I + \frac{1}{2}\sum_i \delta m_i^2 \varphi_i^2 \,. \end{gathered} \tag{1.33}$$

The main point is now in the cancellation occurring between the thermal counterterms from the new interaction Lagrangian and those contributions from higher loop diagrams which are of low order in the couplings and require resummation. For example, the sum of the diagrams from fig. 1.3 does not contribute to the field dependent part of the effective potential up to order g^4. Here the dot symbolizes the thermal counterterm. If the thermal counterterm is

considered as increasing the formal loop order by one, all of these diagrams are of three-loop order. Treating the proper three-loop diagrams, i.e. those without self-energy parts, separately, it can be shown that the sum of all three-loop diagrams does not contribute to the desired g^4-potential.

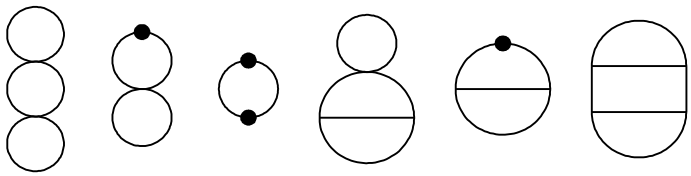

Fig.1.3 Three-loop diagrams with self-energy parts

Arguments of that kind can be generalized to higher loop orders. Therefore, to obtain the full g^4-result in this approach, the diagrams shown in fig. 1.4 are sufficient. Here the circle symbolizes the one-loop contribution which is proportional to the logarithm of the determinant of the propagator. It has to be kept in mind that the notation in this chapter is merely a generic one, so that the lines in the diagrams stand for all the different particles of the theory.

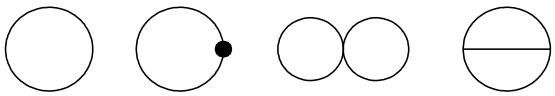

Fig.1.4 Typical diagrams contributing to the g^4-potential in the counterterm method.

In ref. [17] a slight modification of this method is used. There, the resummation is applied only to the zero Matsubara frequency modes. Thereby many constant terms and terms which would cancel each other in the final result are omitted from the beginning. Also, using this method, it is not necessary to keep the dependence on the space dimension in the thermal counterterms, if dimensional regularization is used. The details of this will not be discussed here, because the following calculations are based on the method of section 1.3.1. However, the results of chapters 2 and 3 have been checked by use of the counterterm method.

Chapter 2

Abelian Higgs model

The simplest gauge theory with spontaneous symmetry breaking, the Abelian Higgs model, is believed to exhibit the main features of the electroweak phase transition [35,36]. At one-loop order the effective potential shows a first order phase transition at high temperature, driven by a term cubic in the vector mass in complete analogy to the standard model case [13,14]. The study of the Abelian Higgs model might prove useful for the understanding of the electroweak phase transition, because this simple model does not suffer from the severe infrared problems of the non-Abelian theory. No magnetic mass is expected to arise. This does not present a problem due to the absence of the higher-loop non-Abelian contributions, which are divergent in the symmetric phase.

In this chapter a complete calculation up to the order e^4, λ^2, with gauge coupling e and scalar coupling λ, is presented, supplying the results of ref. [17] with scalar corrections. An analysis of the phase transition parameters shows that these corrections are important if the Higgs mass is not too small.

2.1 Calculation of the potential

The effective potential is calculated by expanding it in the coupling constants, as described in section 1.3.1. Consider the Euclidean Lagrangian

$$\mathcal{L} = -\frac{1}{4}F_{\mu\nu}F_{\mu\nu} - |D_\mu \Phi|^2 + \nu|\Phi|^2 - \lambda|\Phi|^4, \tag{2.1}$$

with

$$D_\mu = \partial_\mu + ieA_\mu \quad \text{and} \quad \Phi = \frac{1}{\sqrt{2}}(\hat{\varphi} + \varphi + i\chi). \tag{2.2}$$

Using the tree level vacuum expectation value v the Higgs mass term is rewritten as $\nu = \lambda v^2$ and counted as order λ. Then the identification with the the generic coupling g of section 1.3

reads $g \sim e \sim \sqrt{\lambda}$. At this point it is necessary to describe in more detail the resummation procedure for the vector particle [14,23]:

The choice of the Landau gauge, which will be used throughout this investigation, is justified by the absence of vector – Goldstone boson mixing together with the φ-independence of the gauge. Two-loop calculations for the three-dimensional model do also show that the convergence of the perturbation series is best in Landau gauge [37]. The bare propagator can be given in the form

$$D_0(k) = \frac{1}{k^2 + m^2}(P_L + P_T)\,, \tag{2.3}$$

where

$$P_{T\,\mu\nu} = \sum_{i,j=1}^{3} \delta_{\mu i}\left(\delta_{ij} - \frac{k_i k_j}{\vec{k}^2}\right)\delta_{j\nu} \quad \text{and} \quad P_{L\,\mu\nu} = \delta_{\mu\nu} - \frac{k_\mu k_\nu}{k^2} - P_{T\,\mu\nu}. \tag{2.4}$$

Here the full covariance has been broken down to SO(3), which is the symmetry left after the specification of a rest frame intrinsic in the formalism of thermal field theory. In ref. [14] the full propagator is shown to have the form

$$D(k) = \sum_{n=0}^{\infty} D_0(k)[\Pi(k)D_0(k)]^n = \frac{1}{k^2 + m^2 + \Pi_L(k)}P_L + \frac{1}{k^2 + m^2 + \Pi_T(k)}P_T\,, \tag{2.5}$$

thus permitting a simple derivation of the mass corrections from the self-energy $\Pi(k)$. Note that P_L and P_T are orthogonal projection operators.

Now the calculation of the different contributions to the potential, listed in eq. (1.28), will be described in some detail. This is possible due to the extreme simplicity of the model. The explicit results are found in appendix B.1. Throughout this investigation dimensional regularization is used. This means that the naively three dimensional parts of the integral-sums are evaluated in $n - 1 = 3 - 2\epsilon$ dimensions. This section together with the relevant parts of the appendix describe the calculation of the $\overline{\text{MS}}$-potential which will be improved by the zero-temperature renormalization of section 2.2.

The first step is the calculation of the leading order temperature corrections to the masses. Here basically the results of ref. [14] have to be supplemented with the ϵ-dependent parts which produce finite contributions to the potential due to one-loop divergences. The results, which can be obtained using the integrals of appendix A.1, are given in appendix B.1.

Consider the contribution V_R first. Due to the particle content of the theory, given by Higgs particle, Goldstone boson, transverse and longitudinal vector boson, the first term of eq. (1.27) reads

$$V_{R1} = \frac{1}{2}\left\{\int dm_\varphi^2 I(m_\varphi) + \int dm_\chi^2 I(m_\chi) + (2 - 2\epsilon)\int dm_T^2 I(m_T) + \int dm_L^2 I(m_L)\right\}\,, \tag{2.6}$$

with the standard temperature integral

$$I(m) = \sum\!\!\!\!\!\!\int dk \frac{1}{k^2 + m^2} \,. \tag{2.7}$$

Similarly, the second term of eq. (1.27) is given by

$$V_{R2} = -\frac{1}{2}(2 - 2\epsilon)\Pi_{b2,T}\, I(m_T) - \frac{1}{2}\Pi_{b2,L}\, I(m_L) \,. \tag{2.8}$$

Note, that this type of corrections does only exist for the vector particles and that $\Pi_{a2}(k) = 0$ in the case of the Abelian model. The sum of both terms $V_R = V_{R1} + V_{R2}$ enters the contribution V_4 which can be found in appendix B.1.

The two-loop contributions of V_z are of vector-scalar and of scalar-scalar type. Figure 2.1 shows the setting sun diagrams of the Abelian Higgs model, contributing to $V_\ominus$. The labelling follows the standard model case. As usual, dashed and wavy lines represent scalar and vector propagators respectively. When solving the integrals, it is useful to write the propagator as a sum of a covariant part and a longitudinal correction

$$D(k) = D_0(k) + \left(\frac{1}{k^2 + m_L^2} - \frac{1}{k^2 + m^2} \right) P_L \,. \tag{2.9}$$

This is possible, because the transverse mass receives no leading order temperature correction, due to gauge invariance.

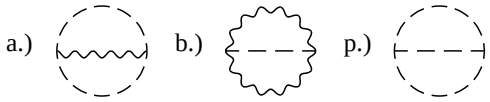

Fig.2.1 Setting sun diagrams in the Abelian Higgs model

A straightforward calculation of all the terms described above results in the explicit formulae given in the appendix.

The necessary $\overline{\rm MS}$-counterterms are generated by a multiplicative renormalization of couplings, mass term and scalar field

$$\lambda_b = Z_\lambda \lambda \quad , \quad e_b^2 = Z_{e^2}\, e^2 \quad , \quad \nu_b = Z_\nu \nu \quad , \quad \Phi_b^2 = Z_{\varphi^2}\, \Phi^2 \,, \tag{2.10}$$

where the index b denotes the bare parameters. No renormalization of the vector field is required because it does not enter the final formula for the potential. The counterterms for the potential are now easily obtained by expressing the bare parameters, which enter the

order g^2, λ part of the potential, through the $\overline{\rm MS}$-quantities, defined by eq. (2.10). Note that the corrections $\delta Z = Z - 1$ are defined to have no finite part. They are given explicitly in appendix B.1 together with the correction to the potential which they generate.

2.2 Renormalization at $T = 0$

To get rid of the arbitrary scale $\bar{\mu}$ the potential is rewritten in terms of physical parameters defined at zero temperature. Such parameters are the Higgs and vector masses and the vacuum expectation value of the physical Higgs field $\varphi^2_{phys} = Z^{-1}_{\varphi^2}\varphi^2_b$. Note that here, in contrast to the $\overline{\rm MS}$-definitions of the previous section, the counterterms δZ do have finite parts, to be specified below.

Returning for the moment to Minkowski space, the usual on-shell definitions of field renormalization factor, Higgs mass and vector mass read

$$Z_{\varphi^2} - 1 = \frac{\partial}{\partial q^2}\mathrm{Re}\ \Pi_\varphi(q^2)\Big|_{q^2=m^2_\varphi}\,, \tag{2.11}$$

$$m^2_\varphi + \mathrm{Re}\ \Pi_\varphi(m^2_\varphi) = m^2_{\varphi,phys} \quad , \quad m^2 + \mathrm{Re}\ \Pi(m^2) = m^2_{phys}\,.$$

They are completed by the specification of the vacuum expectation value v

$$\left.\frac{\partial V}{\partial \varphi_{phys}}\right|_{\varphi_{phys}=v} = 0\,, \tag{2.12}$$

where the Landau gauge zero temperature effective potential to the order e^4, λ^2 is given by

$$\begin{aligned} V = V_{tree} + V_1 \;\; = \;\; & -\frac{\nu_b}{2}\varphi_b^2 + \frac{\lambda_b}{4}\varphi_b^4 - \frac{m_\chi^4}{64\pi^2}\left(\frac{1}{\epsilon} + \frac{3}{2} + \ln\frac{\bar{\mu}^2}{m_\chi^2}\right) \\ & -\frac{m_\varphi^4}{64\pi^2}\left(\frac{1}{\epsilon} + \frac{3}{2} + \ln\frac{\bar{\mu}^2}{m_\varphi^2}\right) - \frac{3m^4}{64\pi^2}\left(\frac{1}{\epsilon} + \frac{5}{6} + \ln\frac{\bar{\mu}^2}{m^2}\right). \end{aligned} \tag{2.13}$$

The one-loop self-energies of Higgs particle and vector field in Landau gauge are given in appendix C.1. Note that in this approach, no one-particle reducible tadpole contributions need to be considered because they vanish due to eq. (2.12).

Requiring the validity of the tree-level relations

$$m^2_{\varphi,phys} = 2\lambda v^2 \quad , \quad m^2_{phys} = e^2 v^2 \quad , \quad \nu = \lambda v^2 \tag{2.14}$$

at one-loop, the above equations permit a straightforward derivation of the necessary counterterms:

$$\delta Z_{\varphi^2} = \mathrm{Re}\,\Pi'_\varphi(m_\varphi^2) \quad , \quad \delta Z_\lambda = -\mathrm{Re}\,\Pi'_\varphi(m_\varphi^2) + \frac{1}{2\nu}\left(\frac{1}{v}V_1'(v) - \mathrm{Re}\,\Pi_\varphi(m_\varphi^2)\right) ,$$

$$\delta Z_\nu = \frac{1}{2\nu}\left(\frac{3}{v}V_1'(v) - \mathrm{Re}\,\Pi_\varphi(m_\varphi^2)\right) \quad , \quad \delta Z_{e^2} = -\mathrm{Re}\,\Pi'_\varphi(m_\varphi^2) - \frac{1}{m^2}\mathrm{Re}\,\Pi(m^2). \tag{2.15}$$

The correction to the potential can now be obtained by renormalization of its leading order part, i.e. by inserting these counterterms into eq. (B.3). This results in a potential, explicitly independent of the renormalization scale $\bar{\mu}$. However, in view of the principal features of the potential considered here, the numerical effect of the performed finite renormalization is not very important (see fig. 2.4).

2.3 Absence of a linear term

In the early days of the perturbative treatment of the phase transition in the U(1)- and SU(2)-Higgs models, the possibility of a linear φ-term in the order-g^3-potential has been discussed. It has however been realized that no such term is present, if the resummation is performed correctly [14, 38–40]. Of course, in the present calculation the cancellation of linear mass terms to order g^3 is reproduced. These terms are not displayed in the final formulae in the appendix to make them more compact.

However, the presence of linear terms in higher orders has not been completely clarified before. Their cancellation is claimed in ref. [40] in a variational approach and in ref. [38] by some gauge invariance argument which is not further specified. Therefore it is interesting to observe that in the present result the linear φ-terms cancel to order g^4: Consider the explicit formulae of appendix B.1 at temperatures above the barrier temperature T_b defined by the vanishing of the φ-independent scalar mass term. Expanding these expressions in φ at the point $\varphi = 0$, linear terms are found in V_a and V_z, which cancel each other exactly. This feature, formulated more precisely as

$$\lim_{\varphi\to 0}\frac{\partial V}{\partial\varphi} = 0 \qquad \text{to all orders in } e \text{ and } \lambda\,,$$

can be shown to survive to all orders of small couplings resummed perturbation theory. The proof is based on an identity following from global U(1)-symmetry:

$$\frac{1}{\varphi}\frac{\partial V}{\partial\varphi} = m_\chi^2(q^2 = 0) \quad . \tag{2.16}$$

Obviously it suffices to demonstrate the finiteness of the self energy $\Pi_\chi(q^2 = 0)$ in the limit $\varphi \to 0$. Due to the positive temperature masses of χ and φ singularities can only arise from the transverse gauge boson propagator above the barrier temperature. Therefore diagrams of the kind shown in fig. 2.2 have to be investigated. Here the wavy lines symbolize leading order resummed vector propagators and the blobs are full vertices without internal vector lines, meaning the sum of all diagrams built from scalar propagators with the correct number of external vector lines and possibly one or two χ-lines. Notice that the vector resummation affects only the longitudinal modes, and is therefore irrelevant for the discussion of small-φ singularities.

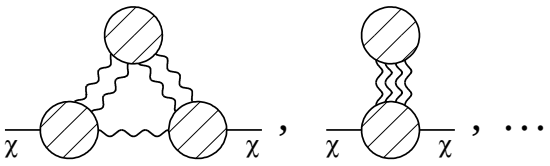

Fig.2.2 Higher loop self-energy corrections to m_χ^2

Consider first the full vertices with external vector lines only denoted by

$$\Gamma^{2n}_{\alpha\beta\ldots\mu\nu}(k_1, \ldots, k_{2n}, \varphi) \tag{2.17}$$

below. Since in the contributing diagrams all propagating particles are massive scalars, the vertices Γ are analytic in k_i.

Above the barrier temperature scalar masses are analytic in φ^2. In addition, explicit φ-factors appearing at the vertices of some diagrams are always paired, due to the structure of the unbroken theory, which has no vertices with an odd number of scalar lines. This shows that Γ is also analytic in φ^2.

Furthermore the three-dimensional part of Γ with vanishing external Matsubara frequencies satisfies

$$\Gamma^{2n}_{\alpha\beta\ldots\mu\nu}(k_1, \ldots, k_{2n}, \varphi = 0) \;\sim\; |\vec{k}_1| \ldots |\vec{k}_{2n}| \tag{2.18}$$

$$\text{for small} \quad |\vec{k}_i| \qquad \text{and} \quad k_i^0 = 0\,, \quad \alpha\beta\ldots\mu\nu \in \{1,2,3\}\,.$$

This follows from a gauge covariance argument, completely analogous to the zero temperature case. Having established these properties of Γ, the small-φ behaviour of the χ-self-energy can be derived as follows:

Consider the most dangerous lowest power of φ stemming from the maximal infrared divergence, which is obtained by setting $k^0 = 0$ for all transverse vector propagators. It can be calculated by scaling the loop momenta according to $\vec{k} \to \vec{k}\varphi$. The above discussion of the pure vector vertices Γ shows that after this scaling they can be counted as order φ^2 at least. In the case where no scalar line connecting two external χ-lines exists (see the first diagram of fig. 2.2), the power counting in φ proceeds as follows: a factor φ^3 for each of the L loops, φ^{-2} for each of the I internal vector lines, φ^2 for each of the $V-2$ full vector vertices and an explicit factor φ for each of the two vertices with a χ-line. Together this gives the minimal over all power of φ

$$n_\varphi = 3L - 2I + 2(V-2) + 2 \tag{2.19}$$

for a diagram with V vertices (compare the argumentation in appendix A of ref. [16]).

If there is at least one scalar line connecting the two external χ-lines (compare the second diagram of fig. 2.2), $V-1$ full vector vertices contribute factors φ^2. In this case however the last term $+2$ does not exist because a vertex with two χ-lines need not have an explicit φ-factor. Therefore eq. (2.19) is valid in the second case as well and consequently in general.

Now the well-known formula $V + L - I = 1$ immediately gives

$$n_\varphi = L \geq 0\,, \tag{2.20}$$

or equivalently: There is no divergence for $\varphi \to 0$.

If some of the vector propagators have non-zero Matsubara frequencies, the vertices connected by those "heavy" lines may be formally fused. Now repetition of the above argument leads again to the desired result, thus completing the proof.

This nice feature of the Abelian model strongly supports the hope for a reliable perturbation series in the symmetric phase. Unfortunately, due to the 3- and 4-vector vertices of the non-Abelian theory, the above argument does not apply there.

2.4 Numerical results and discussion

For the numerical investigation of the phase transition standard model values are chosen for vacuum expectation value v and vector boson mass m_W at zero temperature (see section 3.3.1). Of course the analogy has to be used with caution, because even at one-loop level, the three vector degrees of freedom of the SU(2) increase the strength of the phase transition considerably if compared to the U(1) case. Nevertheless, assuming the standard

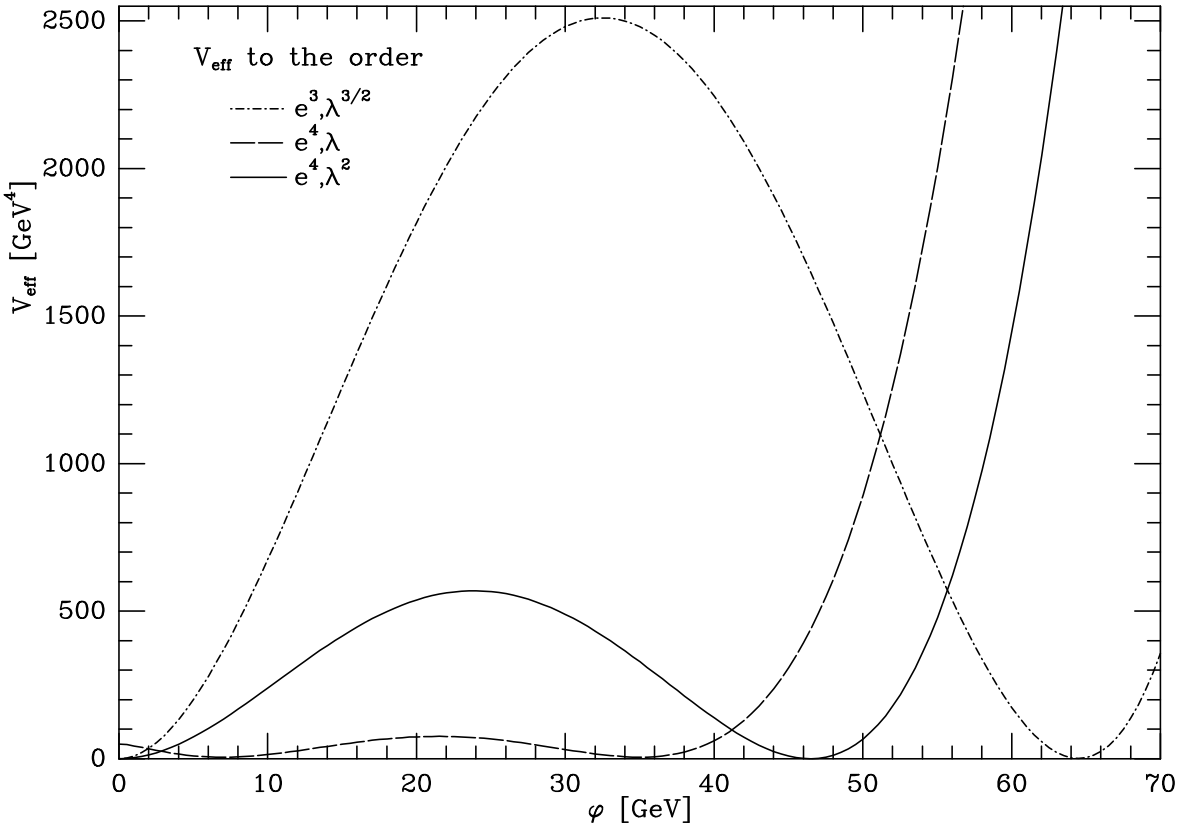

Fig.2.3 Different approximations of the effective potential plotted at their respective critical temperatures at $m_{\text{Higgs}} = 38$ GeV (the e^4, λ-potential is a result of ref. [17])

model situation, in the following analysis the Higgs mass will be considered as an unknown parameter.

As is well known, the potential suggesting a first order phase transition is generated at order $g^3, \lambda^{3/2}$ by the combination of quadratic, cubic and quartic φ-terms, where the coefficient of the quadratic term is of the form $T^2 - T_b^2$ and therefore strongly depends on the temperature (see V_3 in appendix B.1). Figure 2.3 shows the different approximations to the potential at their respective critical temperatures and $m_{\text{Higgs}} = 38$ GeV, all of them suggesting a first order phase transition, but of quite different strength. Calculations of order $e^3, \lambda^{3/2}$ [13,14], of order e^4, λ [17] and the present e^4, λ^2-calculation [19] are compared, showing a dramatic decrease of the barrier height in both higher order results.

Obviously, reliability of perturbation theory has to be questioned already at this small Higgs mass. A more detailed picture can be obtained by considering the surface tension [41]

$$s = \int_0^{\varphi_+} d\varphi \sqrt{2V(\varphi, T_c)}\,, \tag{2.21}$$

which may be seen as a measure of the strength of the phase transition. The reliability of

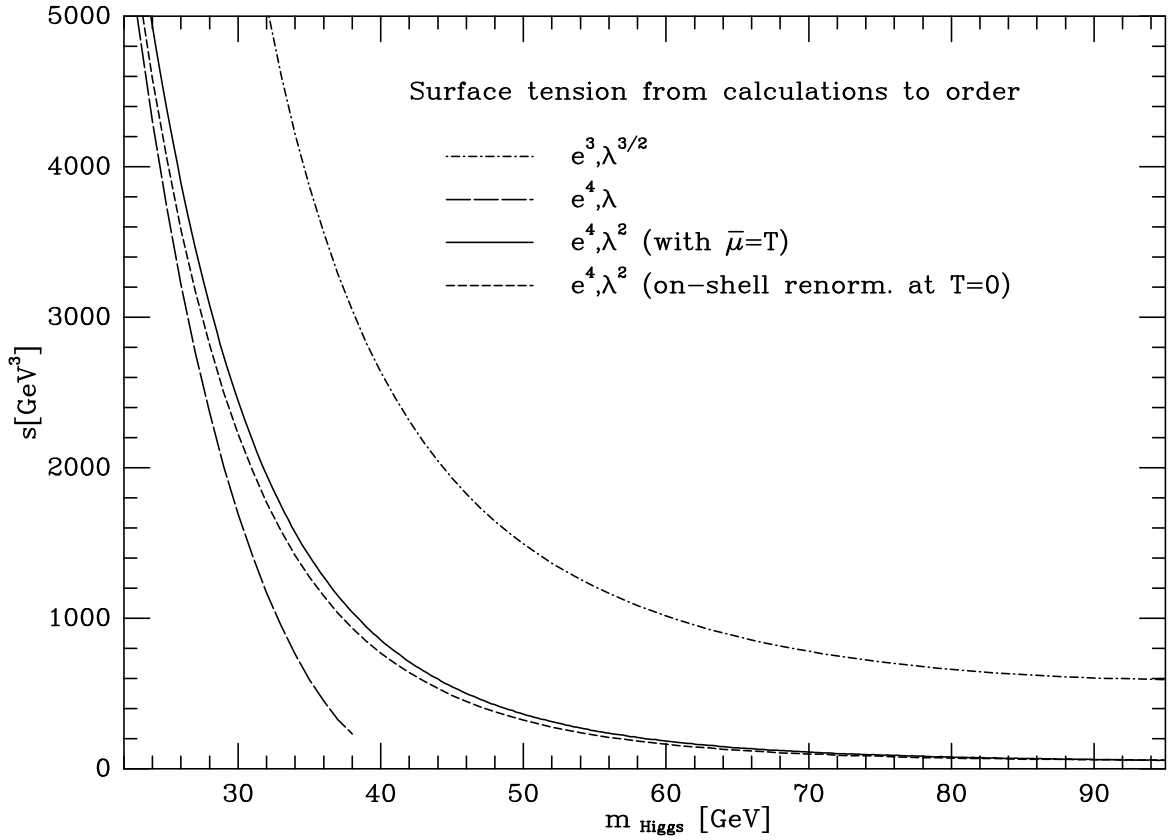

Fig.2.4 Dependence of the surface tension calculated from the different potentials on the zero temperature Higgs mass

the present calculation of this quantity is of course doubtful, because it relies essentially on the non-convex region of the potential, where the physical interpretation is still unclear. Nevertheless s can be used conveniently to discuss the properties of the potential as a function of the Higgs mass. The results are shown in fig. 2.4.

The reasons for the difference between the $e^3, \lambda^{3/2}$ and the e^4, λ^2-results are twofold. Consider the region of small Higgs masses first. Here the $e^4\varphi^4$-term, being a large correction to the tree-level term $\lambda\varphi^4/4$, is mainly responsible for the decrease of the barrier height. This is illustrated in fig. 2.5, where in addition to the consistent third and fourth order results a potential containing the third order terms together with the $e^4\varphi^4$-correction (see V_4 in appendix B.1) is investigated. The effect is not removed by zero temperature renormalization, although the temperature independent constant c_1 forms the largest part of the coefficient of $e^4\varphi^4$. Notice that this large constant arises from the expansion of the temperature dependent part of the one-loop integral $I(m)$ [42], and is therefore absent at $T = 0$.

As it can be seen from fig. 2.5, two-loop contributions are not too important at small

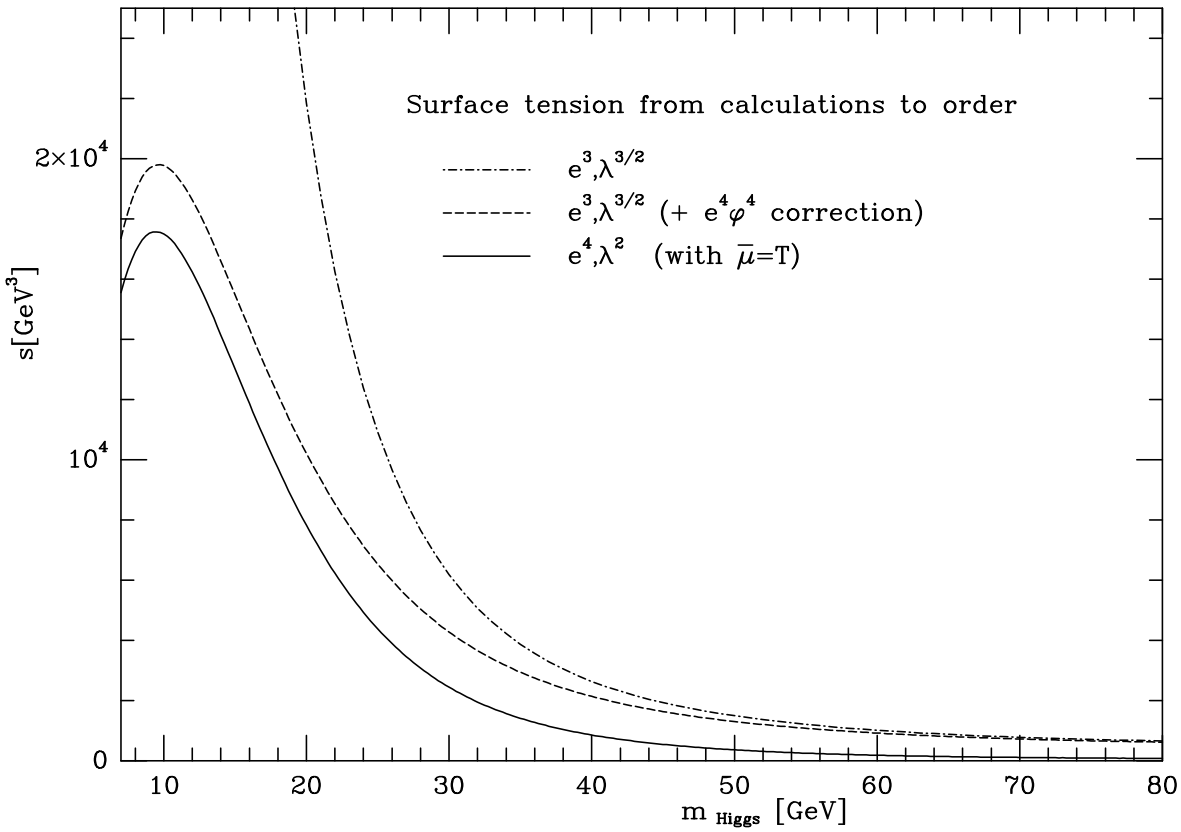

Fig.2.5 Influence of the $e^4\varphi^4$-correction on the surface tension at small Higgs masses

Higgs mass and perturbation theory appears to be in a relatively good shape.

For Higgs masses above ≈ 30 GeV another higher order effect becomes more important: The three-dimensional pieces of two-loop temperature integrals generate terms of the form $\varphi^2 \ln(m + m_{\varphi,\chi})$ and the like (see V_a and V_b in appendix B.1), which, in spite of their numerical smallness, influence the potential significantly. This can be understood by recalling that at the critical temperature the leading order φ^2-terms essentially cancel and that a φ-dependence in a coefficient of φ^2 can not be absorbed in a correction of T_c. These logarithmic terms with a positive sign decrease the barrier height, which is clear from the shape of the function $x^2 \ln(x + \text{const.})$. In summary, the most infrared sensitive contributions of the high temperature field theory introduce large corrections and prevent the reliability of perturbation theory.

The effect of the above logarithmic terms is overestimated by the approximation used in ref. [17]. There, scalar masses are counted as order $\lambda^{1/2}$ and neglected systematically against vector masses, resulting in contributions of the type $\varphi^2 \ln m$. These terms, lacking the scalar mass cutoff in the logarithm, destroy the first order phase transition for Higgs masses above

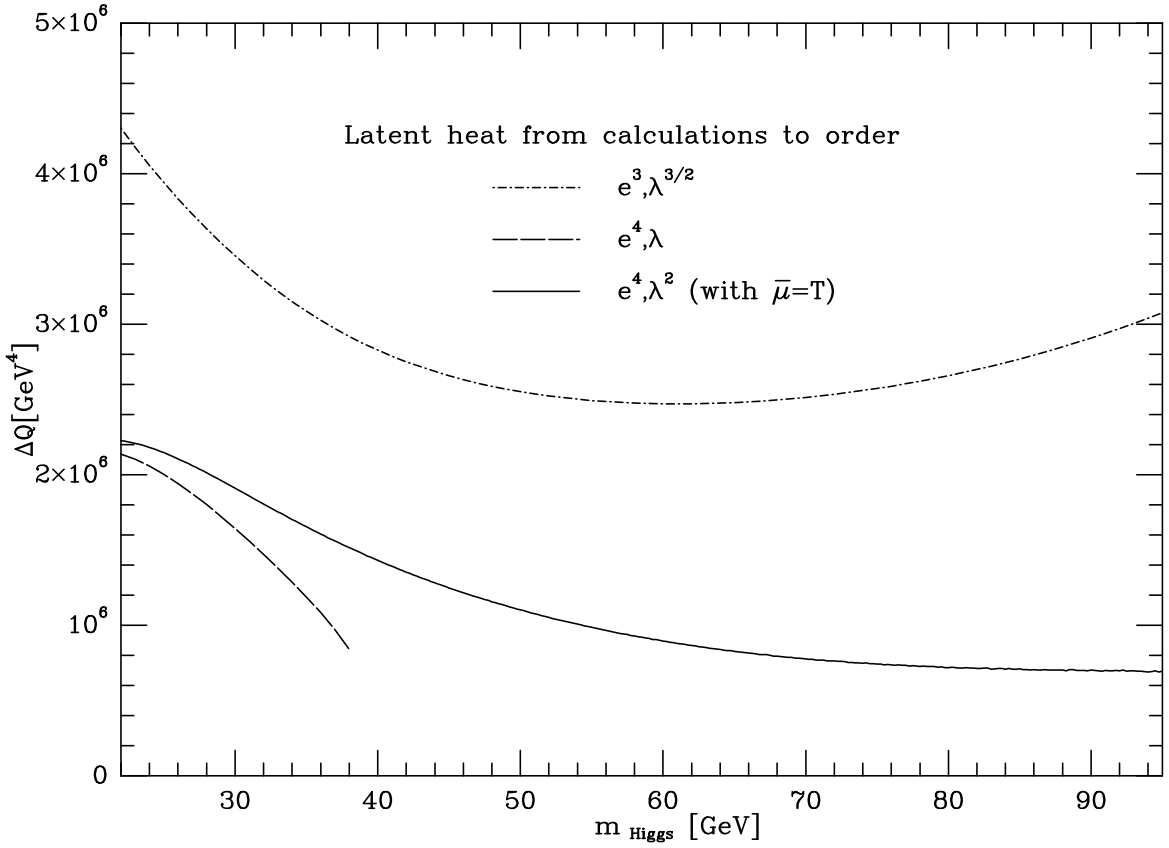

Fig.2.6 Higgs mass dependence of the latent heat ΔQ of the phase transition

$\approx$ 40 GeV. The plot at 38 GeV of fig. 2.3 does already show the arising pathology of the e^4, λ-potential, which can be somewhat eased but not cured by addition of the $\lambda^{3/2}$ terms.

The latent heat of the phase transition is another interesting quantity to be calculated from the effective potential :

$$\Delta Q = T \frac{\partial}{\partial T} V(\varphi_+, T)\Big|_{T_c}, \tag{2.22}$$

where φ_+ is the position of the asymmetric minimum of the potential V, normalized to zero at the origin. This relation follows easily from the definition of ΔQ together with the formula relating entropy and free energy:

$$\Delta Q = T\Delta S = T(S_{symmetric} - S_{broken}) \quad , \quad S = -\frac{\partial V(\varphi, T)}{\partial T}. \tag{2.23}$$

Figure 2.6 shows that the change of the latent heat, introduced by the g^4, λ^2-corrections, is very large, but not as dramatic as for the surface tension. The phase transition appears to be much weaker first order at two-loop.

The vacuum expectation value in the broken phase at T_c, shown in fig. 2.7, does not reflect the dramatic change of the surface tension, introduced by higher order corrections.

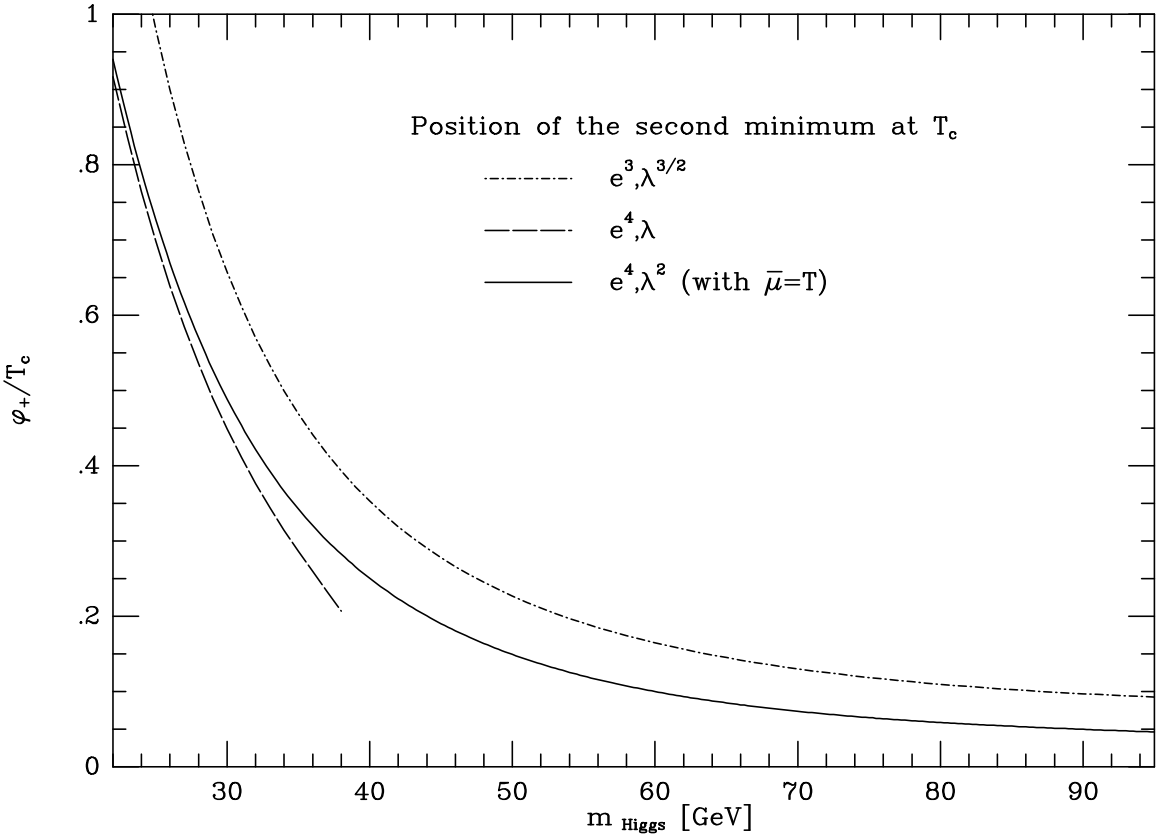

Fig.2.7 Position of the second minimum φ_+ at the phase transition in units of the critical temperature T_c

This quantity, the jump of the order parameter, seems to be the most reliable characteristic of the phase transition, accessible in perturbation theory.

Note that the critical temperature is, here as well as in the standard model case, very close to the uncorrected barrier temperature, defined by the vanishing of the quadratic term in eq. (B.7). Therefore a graphic representation does not seem advisable.

Depending on the considered quantity and the standards to be chosen the phase transition can be regarded as understood in principle for Higgs masses below 30...50 GeV. For larger masses it is likely to be much weaker first order, although even such a qualitative description is not really well founded due to the infrared problems. The next sections will show that reliability at physically relevant large Higgs masses remains a problem in the non-Abelian theory as well.

Chapter 3

Standard model

In the following standard model discussion the technical parts will be confined to the new features not present in the Abelian model. While the non-Abelian character of the theory changes the numerical effect of two-loop corrections qualitatively, fermions and the additional U(1)-symmetry are less important. Therefore it suggests itself to concentrate on the much simpler SU(2)-Higgs model for a detailed analysis of the two-loop effective potential.

This chapter is based on ref. [20].

3.1 Calculation of the potential

To fix the notation the essential parts of the standard model Lagrangian are given:

$$\mathcal{L} = \mathcal{L}_{Higgs} + \mathcal{L}_{gauge} + \mathcal{L}_{fermion} + \mathcal{L}_{Yukawa}. \tag{3.1}$$

Defining the covariant derivative as

$$D_\mu = \partial_\mu + ig_1 \frac{Y}{2} B_\mu + ig_2 \frac{\tau^a}{2} W_\mu^a \tag{3.2}$$

the gauge part and fermionic part for n_f fermion families are unambiguous. The Higgs contribution reads

$$\mathcal{L}_{Higgs} = -|D_\mu \Phi|^2 + \nu|\Phi|^2 - \lambda|\Phi|^4 \quad , \quad \text{where} \quad \Phi = \frac{1}{\sqrt{2}} \begin{pmatrix} \varphi_3 + i\varphi_4 \\ \hat{\varphi} + \varphi_1 + i\varphi_2 \end{pmatrix} \tag{3.3}$$

denotes the Higgs doublet and the shift has been applied according to $\varphi_1 \rightarrow \hat{\varphi} + \varphi_1$. All fermions except the top quark are considered to be massless. The resulting Yukawa Lagrangian is

$$\mathcal{L}_{Yukawa} = -g_Y \bar{q}_L \tilde{\Phi} t_R \,, \qquad q_L = \begin{pmatrix} t_L \\ b_L \end{pmatrix}, \qquad \tilde{\Phi} = i\tau_2 \Phi^*. \tag{3.4}$$

Following section 1.3 the formal power counting rule

$$g_1 \sim g_2 \sim g_Y \sim \lambda^{1/2} \tag{3.5}$$

is used.

The resummation of the scalar and vector degrees of freedom proceeds in analogy to sections 1.3.1 and 2.1. Explicit formulae are found in appendix B.2. The vector resummation is complicated by the mixing of the W_3– and B–fields, characterized by the well known Weinberg angle θ in the transverse part and by a different, temperature dependent angle $\tilde{\theta}$ in the longitudinal part. To implement this in the evaluation of Feynman diagrams the notation of a transverse and longitudinal propagator is introduced:

$$D_T = \frac{1}{k^2 + m^2} P_T \quad , \quad D_L = \frac{1}{k^2 + m_L^2} P_L \,. \tag{3.6}$$

Now the W_3-W_3-propagator is conveniently rewritten as

$$\begin{aligned} D^{W_3 W_3} &= D_T^Z \cos^2\theta + D_T^\gamma \sin^2\theta + D_L^Z \cos^2\tilde{\theta} + D_L^\gamma \sin^2\tilde{\theta} \\ &= D_0^Z \cos^2\theta + D_0^\gamma \sin^2\theta + (cos^2\tilde{\theta} - \cos^2\theta)\left[\left(D_T + D_L^Z\right) - \left(D_T + D_L^\gamma\right)\right] . \end{aligned} \tag{3.7}$$

Here the masses are specified by the indices Z and γ. From this the B-B-propagator is obtained by exchanging sine and cosine. Similarly, the B-W_3-propagator reads

$$D^{BW_3} = \left(D_T^\gamma - D_T^Z\right) \sin\theta\cos\theta + \left(D_L^\gamma - D_L^Z\right) \sin\tilde{\theta}\cos\tilde{\theta} \,. \tag{3.8}$$

Several comments are in order concerning the calculation of V_R. Calculating the first term of eq. (1.27) the ϵ-dependent part of $m_{\gamma L}^4 + m_{ZL}^4$ is needed (compare eq. (2.6)). It is obtained most easily from the last line of eq. (B.18). For the second part of V_R, corresponding to the second term of eq. (1.27), the self energy contribution $\Pi_{a2}(k)$, introduced in eq. (1.21), is required. It is nonzero for the W-field only and can be found in appendix B.2 together with the contributions of type Π_{b2}. These terms are displayed most conveniently in the original B-W_3-basis.

V_z contains two-loop contributions of vector-vector, vector-scalar and scalar-scalar type. The setting sun diagrams are shown in fig. 3.1, where the labelling follows ref. [17], to make comparison more easy.

$$V_\ominus = V_a + V_b + V_i + V_j + V_m + V_p. \tag{3.9}$$

Note that ghost contributions have been included in V_m, and that the purely scalar diagram V_p has not been considered in ref. [17]. The calculation of all these terms is long but

straightforward. All the integrals with complicated covariant structure can be reduced to the basic types given in appendix A.1, as described in ref. [17].

Dropping the appropriate terms of V the lower order g^4, λ-result, as it is given by Arnold and Espinosa in ref. [17], can be derived. This is also valid for the Abelian model discussed in the previous chapter. Another calculation for the SU(2)-Higgs model appeared in ref. [7], where the complete g^4, λ^2 result is derived from the effective three-dimensional theory together with some corrections from ref. [17]. The analytic results of the actual loop-calculation are found to be in agreement with the present analysis. However, due to a specific way to apply the renormalization group method the numerical outcome of ref. [7] differs from the results to be presented here.

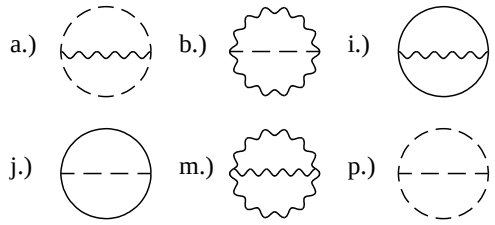

Fig.3.1 Setting sun diagrams for the standard model

Note that there are linear φ-terms of fourth order in the couplings present in V_a, V_m and V_z. As in the Abelian model, these terms cancel each other, thus ensuring the relation $\lim_{\varphi \to 0} \partial V / \partial \varphi = 0$ for all allowed temperatures. This cancellation is essentially the same effect which leads to a vanishing third order transverse gauge boson mass term in the symmetric phase [16], as can be seen in the contributions of diagrams fig. 6.o, 6.q, 6.t and 6.u of ref. [16].

3.2 Renormalization at $T = 0$

In the Abelian Higgs model the performed zero temperature renormalization has not affected the calculated phase transition parameters significantly. Nevertheless, it is not possible to profit from that experience by just setting $\bar{\mu} = 1/\beta$ in the standard model case. The reason for that is the large negative $g_Y^4 \varphi^4$-term which dominates over the tree level quartic term. This leads to an $\overline{\text{MS}}$-potential unbounded from below for small Higgs mass.

The zero temperature renormalization is performed in the on-shell scheme, as described

in ref. [43]. Slightly modifying the procedure of section 2.2, the physical parameters chosen are Higgs mass, top quark mass, W- and Z-boson masses and the fine structure coupling α, defined in the Thompson limit [44]. The physical masses and the wave function renormalization of the Higgs field are defined in analogy to eq. (2.11). A multiplicative renormalization of the coupling constants, the tree level Higgs mass square $-\nu$ and the Higgs field is performed.

The required one-loop corrections are of course well known in Feynman-'tHooft gauge [43]. However, here they are needed in Landau gauge. There is no problem with the correction to the electric charge $\delta e = e_b - e$, which is gauge independent [45]. This can be easily checked explicitly using the results of ref. [46], where the gauge dependence of several self-energy and vertex corrections has been calculated. Therefore in the present calculation the formula for δe from [43] is used. The logarithmic terms with the five light quark masses are treated in the way described in ref. [47], with data from ref. [48], resulting in the vacuum polarization contribution

$$\mathrm{Re}\,\hat{\Pi}^{\gamma(5)}_{\mathrm{had}}(M_Z^2) = \mathrm{Re}\,\Pi^{\gamma(5)}_{\mathrm{had}}(M_Z^2) - \Pi^{\gamma(5)}_{\mathrm{had}}(0) = -0.0282 \pm 0.0009\,. \tag{3.10}$$

The dependence of the one-loop self energy corrections on the gauge parameters has been calculated in ref. [46] for gauge bosons. Therefore the corrections in Landau gauge, needed here, can be taken from [46, 49]. The self energy corrections for the physical Higgs boson and the top quark can be easily calculated in Landau gauge. The results are displayed in appendix C.2.

Defining v as in the Abelian model by eq. (2.12), no one-particle reducible tadpole diagrams need to be added to the self energies. The zero temperature one-loop effective potential $V_{tree} + V_1$, required for that, is easily obtained from eq. (2.13) by including the additional degrees of freedom. The renormalized couplings and the renormalized Higgs mass square are defined by

$$c = \frac{M_W}{M_Z} \quad , \quad cg_1 = sg_2 = e \quad , \quad \lambda = \frac{M_H^2 g_2^2}{8M_W^2} \quad , \quad M_H^2 = 2\nu\,, \tag{3.11}$$

where $s = \sin\theta_W$ and $c = \cos\theta_W$. Now the counterterms follow easily from the definitions of the physical parameters:

$$\begin{aligned}
&\delta Z_{g_1^2} = 2\frac{\delta e}{e} - \frac{\Pi_Z}{M_Z^2} + \frac{\Pi_W}{M_W^2}\,, \quad \delta Z_{g_2^2} = 2\frac{\delta e}{e} + \frac{c^2}{s^2}\frac{\Pi_Z}{M_Z^2} - \frac{c^2}{s^2}\frac{\Pi_W}{M_W^2}\,, \quad \delta Z_{g_Y} = \frac{\delta m_t}{m_t} - \frac{1}{2}\Pi'_\varphi \\
&\delta Z_\lambda = 2\frac{\delta e}{e} + \frac{c^2}{s^2}\frac{\Pi_Z}{M_Z^2} + \frac{s^2-c^2}{s^2}\frac{\Pi_W}{M_W^2} - \frac{\Pi_\varphi}{M_H^2} + \frac{g_2 V_1'}{2M_W M_H^2}\,, \quad \delta Z_\nu = -\frac{\Pi_\varphi}{M_H^2} + \frac{3g_2 V_1'}{2M_W M_H^2}\,.
\end{aligned} \tag{3.12}$$

Here Π and Π' stand for the real parts of the self-energies and their derivatives at the on-shell point.

The renormalized, $\bar{\mu}$-independent potential can now be obtained by applying eqs. (3.12) and the field renormalization $\delta Z_{\varphi^2} = \Pi'_\varphi$ to the leading order contribution, given by the first line of eq. (B.21).

Clearly, the resulting formula for the potential is too long to be given explicitly. However, it seems worthwhile to give the numerically most important parts of the corrections to enable a simplified usage of the analytic result in the appendix. As it has already been mentioned, the main contributions come from the g_Y^4-corrections to parameters of order λ (see also [17]):

$$\delta\lambda = \frac{3g_Y^4}{8\pi^2}\ln\frac{m_t}{\bar{\mu}} \quad , \quad \delta\nu = \frac{3g_Y^4 v^2}{16\pi^2}. \tag{3.13}$$

Introducing these corrections in all terms in the potential contributing to order λ and using standard model tree level relations to calculate the couplings one obtains a result which is 'partially renormalized at zero temperature'. The corresponding correction to the $\overline{\text{MS}}$-potential reads

$$\delta V = \frac{\varphi^2}{2}\left(-\delta\nu + \frac{1}{2\beta^2}\delta\lambda\right) + \frac{\delta\lambda}{4}\varphi^4. \tag{3.14}$$

As it will be seen later (section 3.3.2), the numerical effect of this drastic simplification is not too severe.

3.3 Numerical results and discussion

3.3.1 SU(2)-Higgs model

To obtain an understanding of the qualitative effects of higher order corrections the pure SU(2)-Higgs model is studied first. In this subsection the additional U(1)-symmetry and the effect of fermions are neglected. A discussion of this simplified version is also useful in view of lattice investigations, which deal with the pure SU(2)-Higgs model presently and probably also in the near future.

The relevant potential can be easily derived from the formulae given in the appendix B.2 by performing the limit $g_1, g_Y \to 0$ and setting the number of families n_f to zero. This results in the potential of appendix B.3, which is the basis for the numerical investigation of the present subsection.

Standard model values for W-mass and vacuum expectation value v are used, unless stated otherwise : $M_W = 80.22$ GeV and $v = 251.78$ GeV. The parameter $\bar{\mu}$ of dimensional

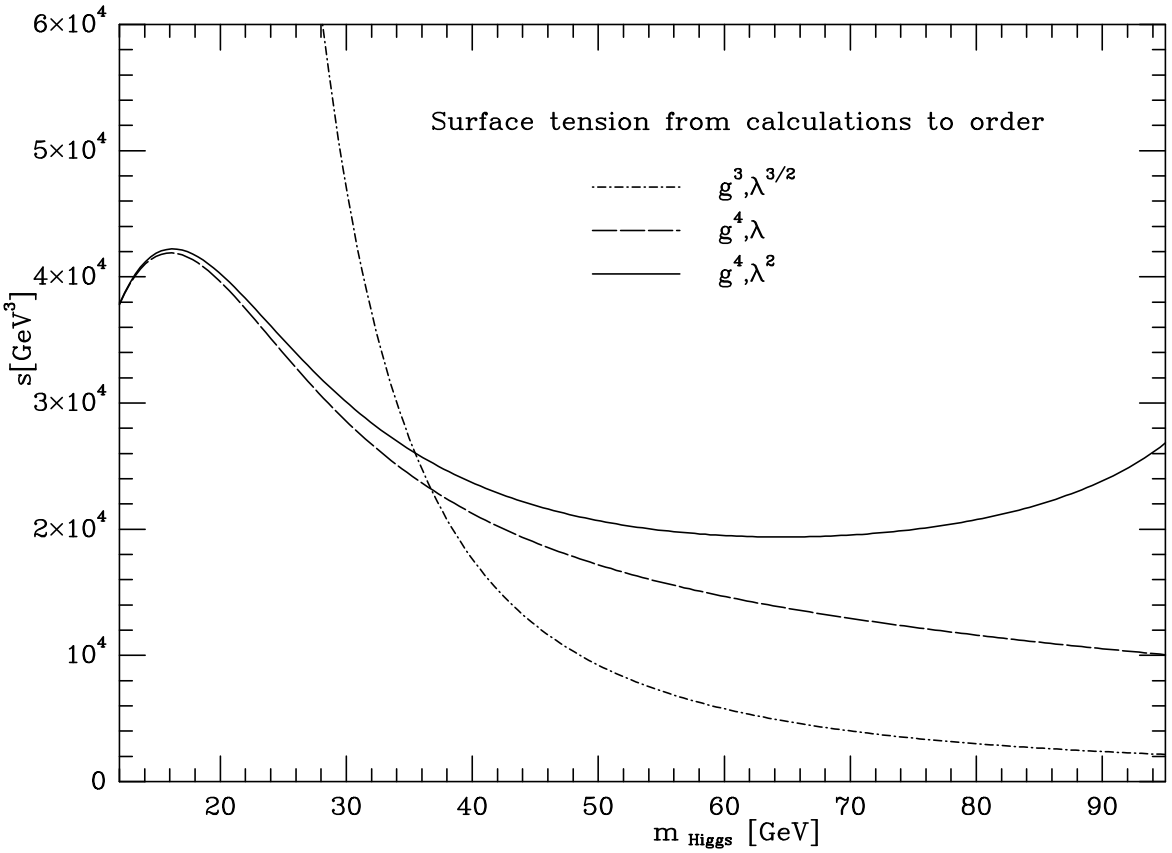

Fig.3.2 The surface tensions calculated from the different potentials as functions of the zero temperature Higgs mass

regularization is set to $T = 1/\beta$. This can be justified by the small dependence on the renormalization procedure. The differences between the results obtained in this scheme and in a scheme with on-shell $T = 0$ renormalization are relatively small. This phenomenon is observed in the Abelian Higgs model as well.

In analogy to the investigation performed in section 2.4 the potentials from calculations to order $g^3, \lambda^{3/2}$ [15,16], to order g^4, λ [17] and to order g^4, λ^2 [20] are compared. All suggest a first order phase transition in a wide Higgs mass range. The form of the potentials at the critical temperature is the standard one (see fig. 2.3) and will not be shown here again. However, comparing the barrier height in the different approximations the picture differs significantly from the Abelian case in the region of large Higgs masses: Both g^4, λ- and g^4, λ^2-potential suggest a much stronger first order phase transition than the lowest order result. The pathological behaviour of the e^4, λ-potential of the Abelian model does not arise.

In the following, the surface tension (see eq. (2.21)) will be used to illustrate the features of the potentials at different Higgs masses. Figure 3.2 shows the similarity of the situations

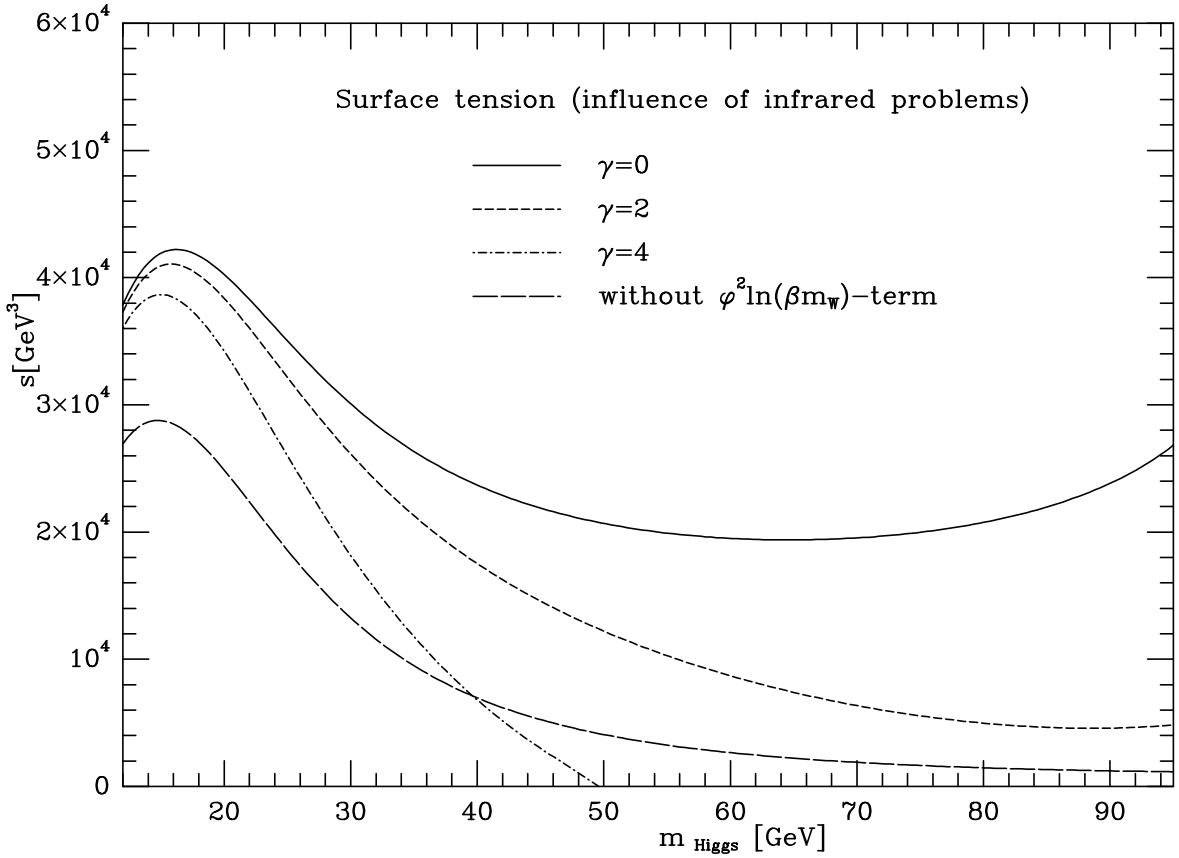

Fig.3.3 Influence of the most infrared sensitive contributions on the surface tension as a function of the Higgs mass

in the Abelian and the non-Abelian case in the small Higgs mass region. The $g^4\varphi^4$-term from the one-loop vector contribution is responsible for the strong decrease of the barrier height in the higher order results.

At larger Higgs masses, approximately above 40 GeV, the infrared two-loop contributions become more important. Their effect is however quite different from the Abelian case. Compare the results of order $g^3, \lambda^{3/2}$ and g^4, λ^2 first. The increase in the strength of the phase transition, studied already in ref. [18], can be traced back to the infrared features of a non-Abelian gauge theory. The crucial contribution is the one coming from the non-Abelian setting sun diagram (fig. 3.1.m). It produces contributions to the potential of type $\varphi^2 \ln(\beta m_W)$ with a negative sign. Recall, that the logarithmic terms from diagrams 3.1.a and 3.1.b (or 2.1.a, 2.1.b), discussed in the Abelian case, have a positive sign. Notice also, that the new terms are non-analytic at $\varphi = 0$. The reason why these kind of corrections affect the form of the potential strongly has already been discussed in section 2.4. To demonstrate its importance the $\varphi^2 \ln(\beta m_W)$-term of V_m has been deleted by hand. The corresponding

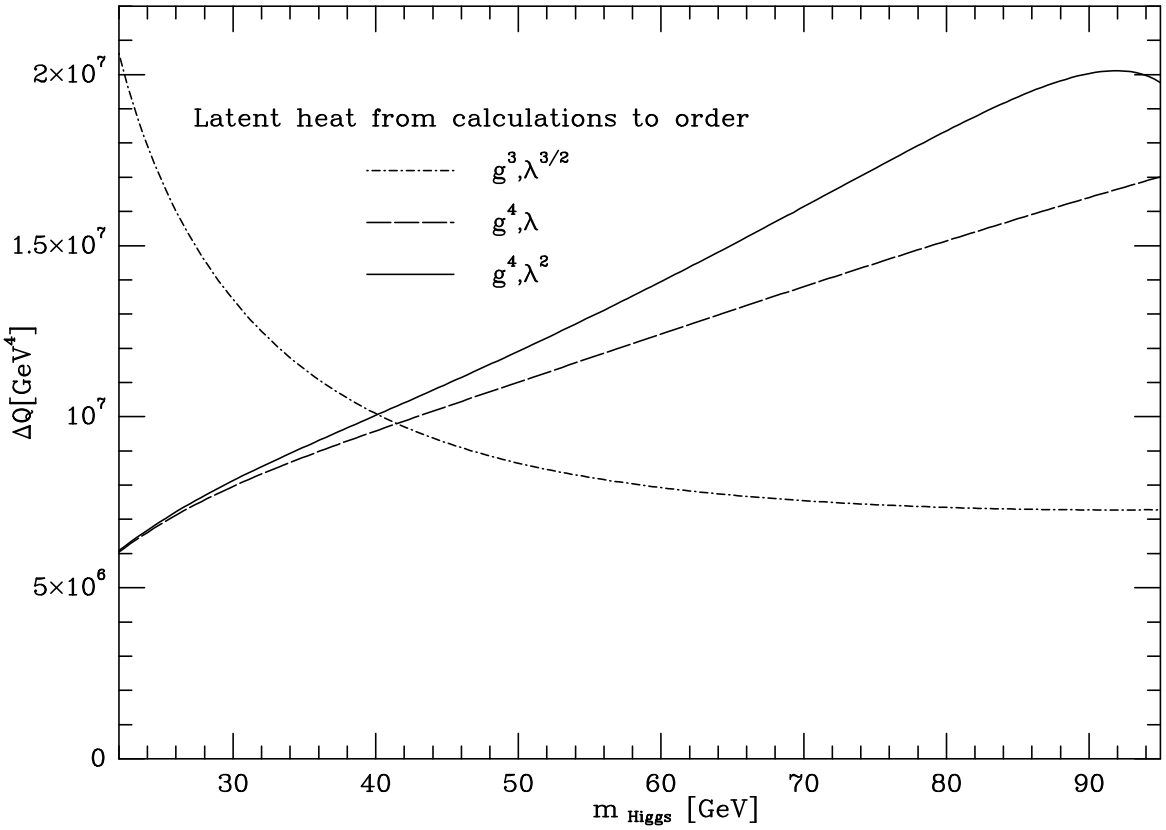

Fig.3.4 Higgs mass dependence of the latent heat ΔQ of the phase transition

surface tension is shown in fig. 3.3 (long-dashed line).

The comparison of the potentials to order g^4, λ [17] and g^4, λ^2 shows a picture very similar to the Abelian Higgs model. Neglecting scalar masses in the logarithms results in spurious $\varphi^2 \ln(\beta m_W)$-terms, which reduce the surface tension. Another important contribution, less significant in the Abelian case, is the one proportional to $g^2(m_1 + 3m_2)m_{WL}$ from V_z. This term comes from scalar-vector diagrams of type of fig. 1.2.b and it was neglected in ref. [17]. On the relevant scale ($\varphi < T$) it produces a very steep behaviour of the potential, again increasing the surface tension. The observed difference between the result of ref. [17] and the complete g^4, λ^2 calculation presented here is mostly due to these two effects, together with the well known influence of the cubic scalar mass contributions from V_3. However, in sharp contrast to the Abelian case, both the g^4, λ- and the g^4, λ^2-calculation suggest a much stronger first order phase transition than the lowest order result.

Another interesting effect of higher order λ-corrections is the complete breakdown of the phase transition at a Higgs mass of about 100 GeV, where the surface tension is very large. In this region the above mentioned term, proportional to $g^2(m_1 + 3m_2)m_{WL}$, becomes

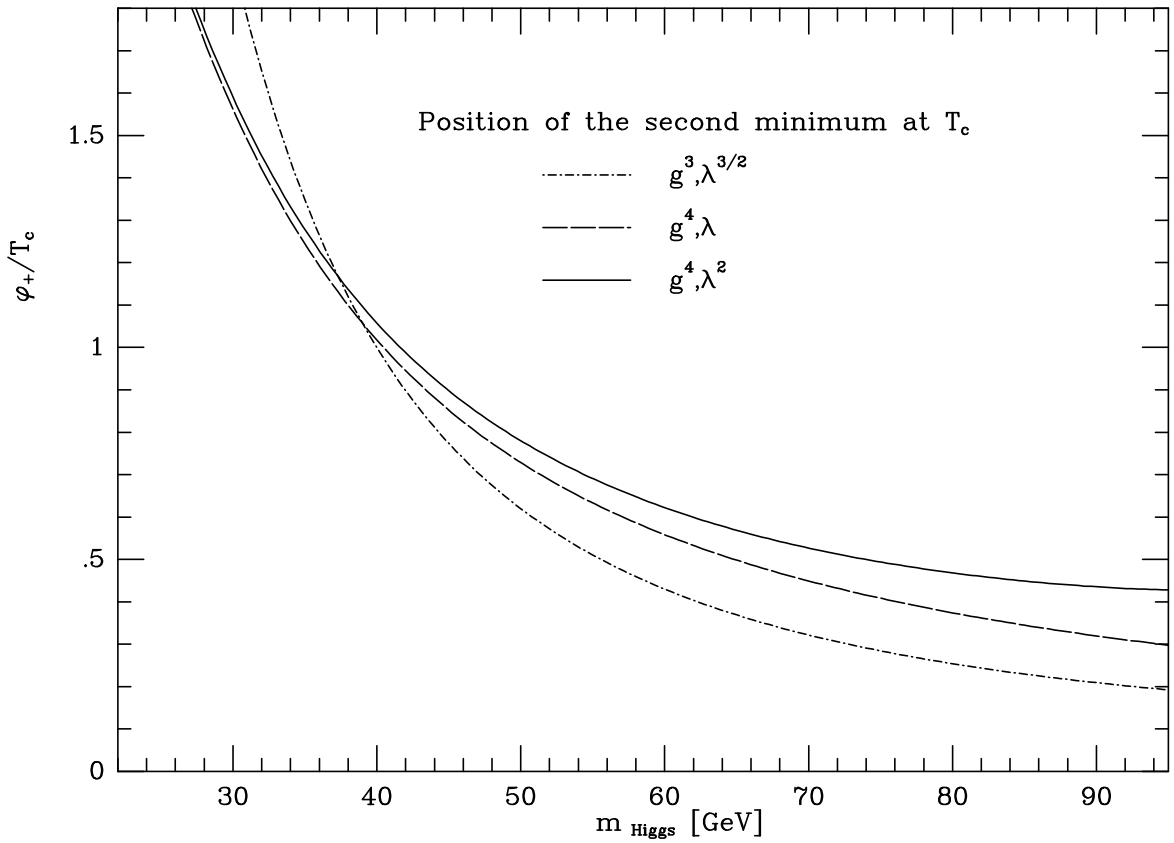

Fig.3.5 Position of the second minimum φ_+ in units of the critical Temperature T_c

important. For a temperature close to the uncorrected barrier temperature T_b, at which the scalar masses vanish for $\varphi = 0$, it produces an almost linear behaviour in the small φ region. This results in a potential for which at $T = T_b$ the asymmetric minimum is not a global minimum but only a local one. Note that T_b is the lowest temperature accessible in this calculation. In other words, the temperature region in which the phase transition occurs can not be described by the given method, due to infrared problems.

In order to illustrate the possible effects of the unknown infrared behaviour of the transverse vector propagator, the dependence of the surface tension on the magnetic mass can be studied. A magnetic mass of order $g^2T/3\pi$ is motivated by the solution of gap equations [16] and supported by the numerical investigation of gauge invariant gap equations with resummed vertices [50]. Following the approach of ref. [16] the transverse vector mass takes the form

$$m_W^2 = \left(\frac{g\varphi}{2}\right)^2 + \left(\frac{\gamma g^2}{3\pi\beta}\right)^2 , \tag{3.15}$$

where γ is some unknown parameter. One can introduce this redefined transverse mass

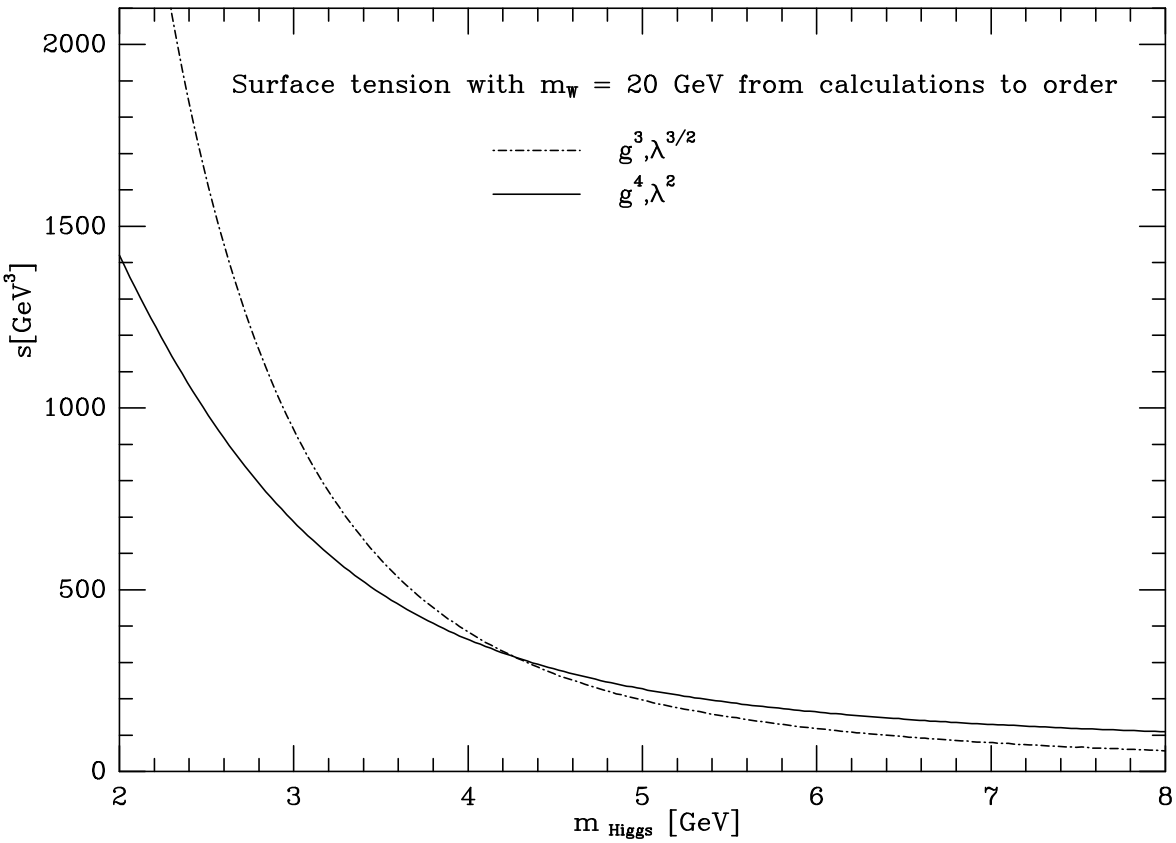

Fig.3.6 Surface tensions from the third and fourth order potentials for a model with $M_W = 20$ GeV in the Higgs mass range where the values differ by a factor of 2 at most

in the most influential infrared contributions, i.e. in the m_W^3- and in the $\varphi^2 \ln \beta m_W$-terms. Figure 3.3 shows the results obtained for $\gamma = 0$, 2 and 4, supporting the qualitative behaviour found in ref. [16]. The main difference is due to the fact that the higher order result suggests a stronger first order phase transition, thus for a given $m_{\rm Higgs}$ a larger magnetic mass is necessary to change the phase transition to second order.

A complete fourth order calculation of the surface tension has to include the wave function correction term $Z_\varphi(\varphi^2, T)$ calculated in ref. [28]. Using the results of ref. [28] the surface tension

$$s = \int_0^{\varphi_+} d\varphi \sqrt{2\,(1 + Z_\varphi(\varphi^2, T))\, V(\varphi, T_c)}\,, \tag{3.16}$$

has been determined for Higgs masses between 25-95 GeV. The numerical effect of this Z-factor is very small, only $1\% - 4\%$. This is due to the smallness of the potential in the only region where Z_φ is significant, i.e. at small φ.

The latent heat ΔQ (see eq. (2.22))is plotted in fig. 3.4 as a function of the Higgs mass. In contrast to the Abelian model, here the higher order results show an almost linear increase of

the latent heat with the Higgs mass. This somewhat surprising behaviour can be understood by observing that for those potentials neither the position of the degenerate minimum nor the height of the barrier change significantly with increasing Higgs mass (see fig. 3.2). Therefore $\partial V/\partial T$ does not change dramatically over a wide Higgs mass range. On the other hand the critical temperature increases with growing $m_{\rm Higgs}$.

As in the Abelian case the quantity φ_+/T_c, shown in fig. 3.5 as a function of the Higgs mass, is least affected by higher order corrections.

Now the question arises whether a good convergence of the perturbation series, which can not be claimed in the whole range of λ for a realistic gauge coupling $g = 0.64$, could be present in the region of much smaller gauge coupling constants. This seems indeed to be the case, as can be seen in fig. 3.6, where the surface tensions of order $g^3, \lambda^{3/2}$ and g^4, λ^2 are plotted for a model with a vector mass of 20 GeV, i.e. $g = 0.16$. In the used Higgs mass range the two results for s differ by a factor of two at most. The relative size of this range, i.e. the ratio of the minimal and maximal values of the Higgs mass, is 4, which is twice as large as the corresponding range for the model with $M_W = 80$ GeV.

The phase transition parameters calculated in this section can be compared to new lattice data available at a low Higgs mass point ($m_{\rm Higgs} \approx 18$ GeV) and a high point ($m_{\rm Higgs} \approx 49$ GeV) [11,12]. These data include critical temperature, jump of the order parameter $\Phi^\dagger\Phi$, latent heat and surface tension at both Higgs mass values. The g^4, λ^2-results are in good quantitative agreement with lattice data (explicit numbers will appear soon [22]). This is highly non-trivial, since quantities change by large factors between low and high point. An exception is formed by the surface tension at the high point, which is larger by a factor of ~ 2.5 in perturbation theory. All other parameters agree between the perturbative and the lattice calculation with deviations compatible with the observed scaling violation on the lattice and the uncertainties of perturbation theory. Note, that the simulations have been performed with a maximum number of three lattice points in time-like direction, thus the results may change somewhat on larger lattices. To obtain the good agreement quoted above the renormalization effect of the vector boson on the very light Higgs particle has to be taken into account at the low point [22].

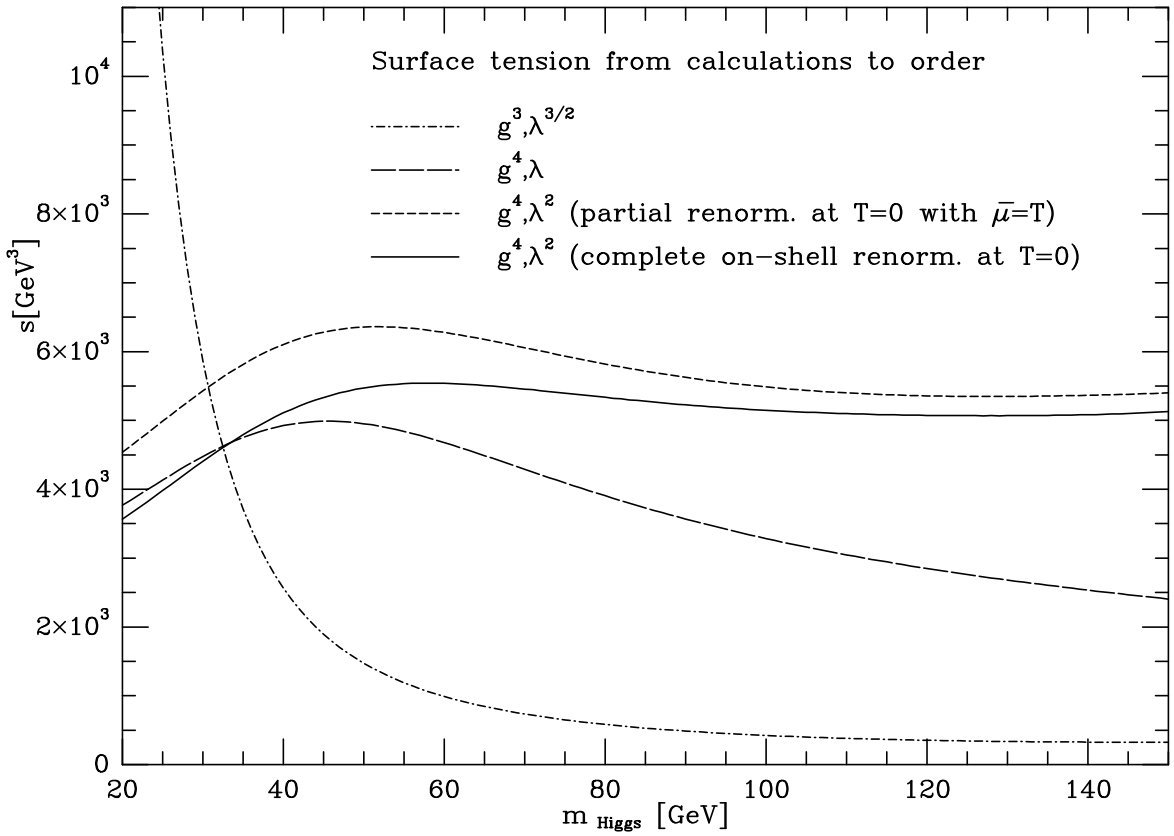

Fig.3.7 The surface tensions obtained from the standard model effective potentials as functions of the zero temperature Higgs mass with $m_{\rm top} = 170$ GeV

3.3.2 Complete standard model

In the case of the full standard model the qualitative behaviour of the potential is essentially the same as for the SU(2)-Higgs model. The main difference is a decrease of the surface tension by a factor ~ 4. This can be traced back to the large top quark mass which influences the potential by lowering the barrier temperature (see B.21). The additional U(1)-symmetry and the light fermions are less important. Also the characteristic points of the surface tension plot of fig. 3.2 are shifted to higher values of the Higgs mass. Figure 3.7 shows the surface tension as a function of $m_{\rm Higgs}$. The complete breakdown of the g^4, λ^2 calculation, observed at $m_{\rm Higgs} \approx 100$ GeV for the pure SU(2) case, occurs at $m_{\rm Higgs} \approx 200$ GeV in the full model. These quantitative differences do not change the qualitative features of the potential, thus the discussion given in the previous section does also apply to the standard model. The difference between the fully renormalized potential and the partially renormalized potential (see eqs. (3.13),(3.14)) is not too severe in view of the huge

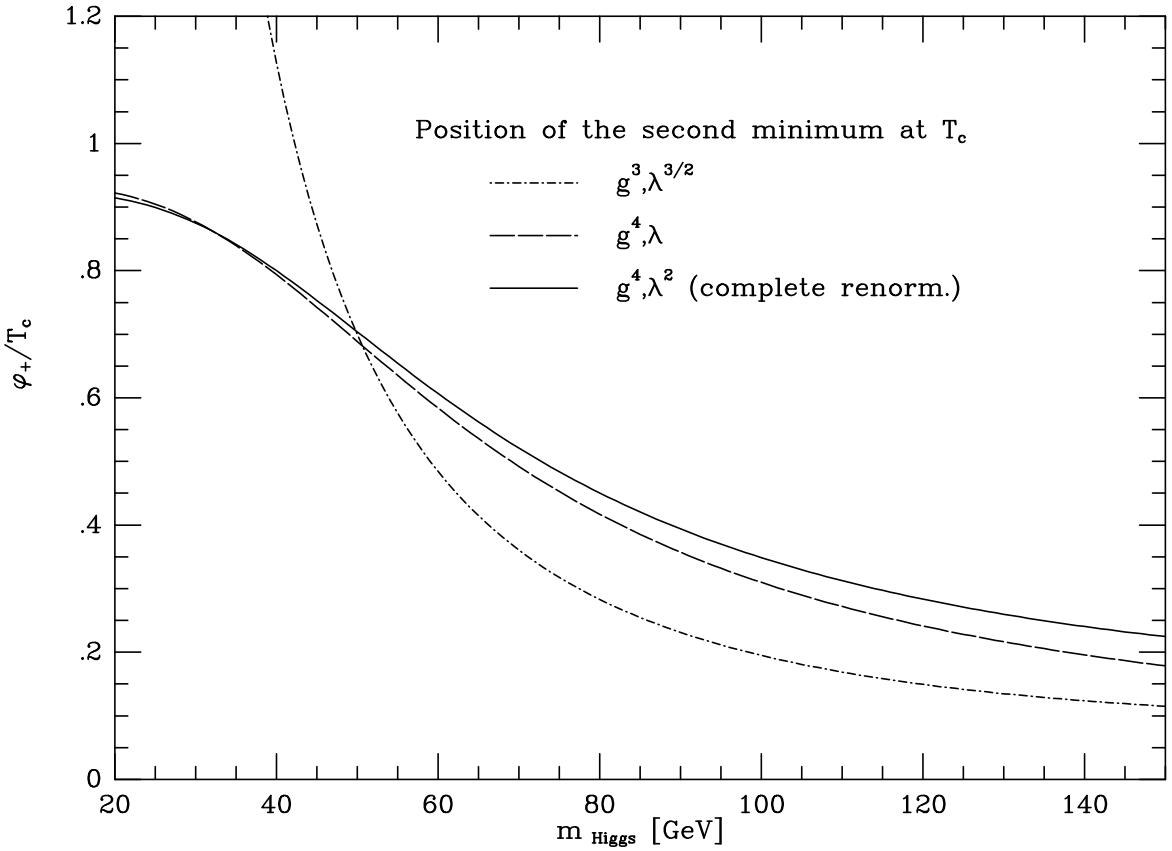

Fig.3.8 Position of the second minimum φ_+ in units of the critical temperature T_c in the case of the standard model with $m_{\rm top} = 170$ GeV

uncertainties still present in the perturbative approach. Again, the position of the second minimum at the critical temperature given in fig. 3.8, does not depend as strongly on the order of the calculation as the height of the barrier. Unfortunately, the region $m_{\rm Higgs} \approx$ 40 GeV, in which the reliability of the perturbative approach is the best and $\varphi_+/T_c \approx 1$, is well below the experimental Higgs mass bound.

Chapter 4

Gauge invariant approach

In this chapter the gauge invariant treatment of the electroweak phase transition is presented following ref. [21]. The main new point is the introduction of a gauge invariant source term [51]

$$Z = \exp(-\beta\Omega W) = \mathbf{tr}\exp\left[-\beta(\boldsymbol{H} + \int_V J\,\boldsymbol{\Phi}^\dagger\boldsymbol{\Phi})\right] \tag{4.1}$$

and the subsequent definition of an effective potential by the Legendre transformation

$$V(\sigma,T) = W(J,T) - J\frac{\sigma}{2} \qquad , \qquad \frac{\sigma}{2} = \frac{\partial W(J,T)}{\partial J}\,, \tag{4.2}$$

which is performed perturbatively. The new variable $\sigma/2 =< \boldsymbol{\Phi}^\dagger\boldsymbol{\Phi} >$ describes the thermal expectation value of a gauge invariant quantity.

This approach is perfectly well suited for comparison with lattice investigations, which usually proceed without gauge fixing and consider the expectation value of the operator $\boldsymbol{\Phi}^\dagger\boldsymbol{\Phi}$. Note also, that effective actions for composite operators have been defined previously, for example in ref. [52], and that a formulation based on a field linearly related to ϕ^2 has been given in ref. [53].

4.1 One-loop calculation of $W(J)$ for the SU(2)-Higgs model

The analysis is restricted to the pure SU(2)-Higgs model, which is sufficient to illustrate the main features of this method at the one-loop level. Note that a comparison with the Abelian model makes no sense at one-loop level since qualitative differences start to appear only at the next loop order. Using the Lagrangian $\mathcal{L}$ from section 3.1, where the appropriate limits have been taken (see section 3.3.1), the thermodynamic potential W can be calculated from

the path integral

$$\exp(-\beta\Omega W) = \int D\Phi D\Phi^\dagger DW_\mu \exp\left[\int_0^\beta d\tau \int d^3\vec{x}(\mathcal{L} - J\Phi^\dagger\Phi)\right] . \tag{4.3}$$

To evaluate this integral the extremum of the static, Φ-dependent part of the action with source term, characterized by V_{tree}, has to be determined:

$$\mathcal{L}^J = \mathcal{L} - J\Phi^\dagger\Phi = -V_{tree} + \cdots , \tag{4.4}$$

$$V_{tree} = (-\nu + J + \alpha_0 T^2)\,\Phi^\dagger\Phi + \lambda(\Phi^\dagger\Phi)^2 . \tag{4.5}$$

Here, following the philosophy described in section 1.3.2, a thermal counterterm for the scalar field has been introduced. Its leading and next to leading order contributions read

$$\alpha_0 = \alpha_{01} + \alpha_{02} = \left(\frac{1}{2}\lambda + \frac{3}{16}g^2\right) - \frac{3g^3}{16\pi}\sqrt{\frac{5}{6}} . \tag{4.6}$$

The g^3-term, generated by the one-loop self-energy contribution of the longitudinal vector boson (see ref. [16], eqs. (41),(42)), is taken into account for reasons to be explained below.

Two different regimes have to be distinguished for the calculation of $W(J)$. Consider the case with $J < \nu - \alpha_0 T^2$ first. In this situation V_{tree} develops a non-trivial minimum at $\varphi_1 = \hat{\varphi}(J)$ (see eq. (3.3) for the conventions), defined by

$$\lambda\hat{\varphi}^2 = M^2 = \nu - J - \alpha_0 T^2 . \tag{4.7}$$

Performing the shift $\varphi_1 \to \hat{\varphi} + \varphi_1$ a tree-level contribution

$$W_{tree}(J) = \frac{1}{2}(-\nu + J)\hat{\varphi}^2 + \frac{\lambda}{4}\hat{\varphi}^4 , \tag{4.8}$$

which is independent of the resummation, is generated. The one-loop contribution in Lorentz gauge (cf. ref. [42]) with gauge fixing parameter α reads

$$W_1(J) = \frac{1}{2}\sum\!\!\!\!\!\!\int dk \left[9\ln(k^2 + m^2) + \ln(k^2 + m_1^2) + 3\ln(k^4 + k^2 m_2^2 + \alpha m^2 m_2^2) - 6\ln k^2\right]$$

$$+ \frac{1}{2}\int \frac{d^3\vec{k}}{(2\pi)^3\beta}\left[3\ln(\vec{k}^2 + m_L^2) - 3\ln(\vec{k}^2 + m^2)\right] . \tag{4.9}$$

Here Higgs mass, Goldstone mass, vector mass and longitudinal vector mass are given by

$$m_1^2 = 2M^2 \quad , \quad m_2^2 = 0 \quad , \quad m^2 = \frac{1}{4}g^2\hat{\varphi}^2 \quad , \quad m_L^2 = \frac{1}{4}g^2\hat{\varphi}^2 + \frac{5}{6}g^2T^2 . \tag{4.10}$$

Note that only the zero Matsubara frequency mode of the longitudinal vector degree of freedom has been resummed. This simplifies the calculation in Lorentz gauge and does not change the result up to order g^3 extracted from the one-loop formula.

If, on the other hand, $J > \nu - \alpha_0 T^2$, no shift of the field is necessary and $W(J)$ has no tree-level contribution. The one-loop term can be easily obtained from eq. (4.9) by setting

$$m_1 = m_2 = M \qquad \text{with} \qquad M^2 = -\nu + J + \alpha_0 T^2 \tag{4.11}$$

and replacing transverse and longitudinal vector masses by zero and $m_{L,0} = \sqrt{5/6}gT$ respectively.

In both the symmetric and the broken phase eq. (4.9) gives explicitly gauge independent results since the product $m_2 m$ is always zero. Working in R_ξ-gauge the same answer is obtained. The integrals are easily performed using appendix A.1 and terms of fourth and higher order in the masses are neglected together with constant terms common to both phases.

The one-loop thermodynamic potential $W(J)$ in broken and symmetric phase is given by

$$W(J) = W_b(J)\Theta(\nu - J - \alpha_0 T^2) + W_s(J)\Theta(-\nu + J + \alpha_0 T^2)\,, \tag{4.12}$$

where

$$\begin{aligned} W_b(J) &= -\frac{T^2}{6}M^2 - \frac{1}{4\lambda}M^4 \\ &\quad -\frac{T}{12\pi}\left[(2M^2)^{3/2} + 6m^3 + 3m_L^3\right] - \frac{\varphi^2}{2}\alpha_{02}T^2\,, \end{aligned} \tag{4.13}$$

$$W_s(J) = \frac{T^2}{6}M^2 - \frac{T}{12\pi}\left[4M^3 + 3m_{L,0}^3\right] \tag{4.14}$$

and M^2 is given by eqs. (4.7) and (4.11) respectively.

4.2 Gauge invariant effective potential

The one-loop gauge invariant effective potential can now be obtained by a perturbative Legendre transformation according to eq. (4.2). In the usual approach, based on the order parameter φ, the perturbatively defined effective potential is the sum of the one-particle irreducible vacuum graphs of the shifted theory. However, no such interpretation is known for the gauge invariant potential $V(\sigma)$. Therefore, after writing $W(J)$ and J as a sum of contributions of increasing order

$$W(J) = W_0(J) + W_1(J) + W_2(J) + \cdots \qquad , \qquad J = J_0 + J_1 + J_2 + \cdots\,, \tag{4.15}$$

the definition (4.2) has to be implemented order by order in perturbation theory [21, 54]. The first terms of the resulting potential are given by

$$V(\sigma) = \left[W_0(J_0) - \frac{\sigma}{2}J_0\right] + \left[W_1(J_0)\right] + \left[W_2(J_0) - \frac{1}{2}\left(\frac{\partial W_1(J)}{\partial J}\Big|_{J_0}\right)^2 \Big/ \frac{\partial^2 W_0(J)}{\partial J^2}\Big|_{J_0}\right] + \cdots , \tag{4.16}$$

where J_0 is a function of σ defined by the leading order relation

$$\frac{\partial W_0(J)}{\partial J}\Big|_{J_0} = \frac{\sigma}{2} . \tag{4.17}$$

Consider the phase with broken symmetry first. Here $W(J)$ has to be decomposed into a leading term W_0 (order g^2, λ) and a next to leading term W_1 (order $g^3, \lambda^{3/2}$), defined by the first and second line of eq. (4.13) respectively.

In the symmetric phase, where no tree-level term exists, the Legendre transformation can be performed exactly at one-loop order. Neglecting constant terms common to both phases the resulting potential is given by

$$V(\sigma) = V_s(\sigma')\Theta(\sigma') + V_b(\sigma')\Theta(-\sigma') \quad , \quad \sigma' = \sigma - \frac{T^2}{3} , \tag{4.18}$$

where

$$\begin{aligned} V_b(\sigma') &= \frac{1}{2}(\alpha_{01}T^2 - \nu)\sigma' + \frac{\lambda}{4}\sigma'^2 \\ &\quad - \frac{T}{12\pi}\left[(2\lambda\sigma')^{3/2} + 6\left(\frac{1}{4}g^2\sigma'\right)^{3/2} + 3\left(\frac{1}{4}g^2\sigma' + \frac{5}{6}g^2T^2\right)^{3/2}\right] , \end{aligned} \tag{4.19}$$

$$V_s(\sigma') = \frac{1}{2}(\alpha_0 T^2 - \nu)\sigma' - \frac{\pi^2}{6}\frac{\sigma'^3}{T^2} - \frac{T}{4\pi}\left(\frac{5}{6}g^2T^2\right)^{3/2} . \tag{4.20}$$

Here the new variable σ' has been introduced to separate the shift of the field variable generated by the interaction from the basic, model independent thermal expectation value $T^2/3$ [35]. Note the similarity of V_b to the order-$g^3, \lambda^{3/2}$ Landau gauge result, eq. (B.31). The new values of the scalar masses, namely zero for the Goldstone boson mass and $2\lambda\sigma'$ for the Higgs mass square, form the main difference of V_b and V_3.

The gauge invariant potential defines a critical temperature at which its two minima, one in the symmetric and one in the broken phase, are degenerate. This is illustrated in fig. 4.1. For comparison, the Landau gauge potential to order $g^3, \lambda^{3/2}$ is plotted at its critical temperature in fig. 4.2. The interaction induced shift σ' seems to play a role similar to the squared field expectation value φ^2 of the usual approach (compare the discussion in section 4.4).

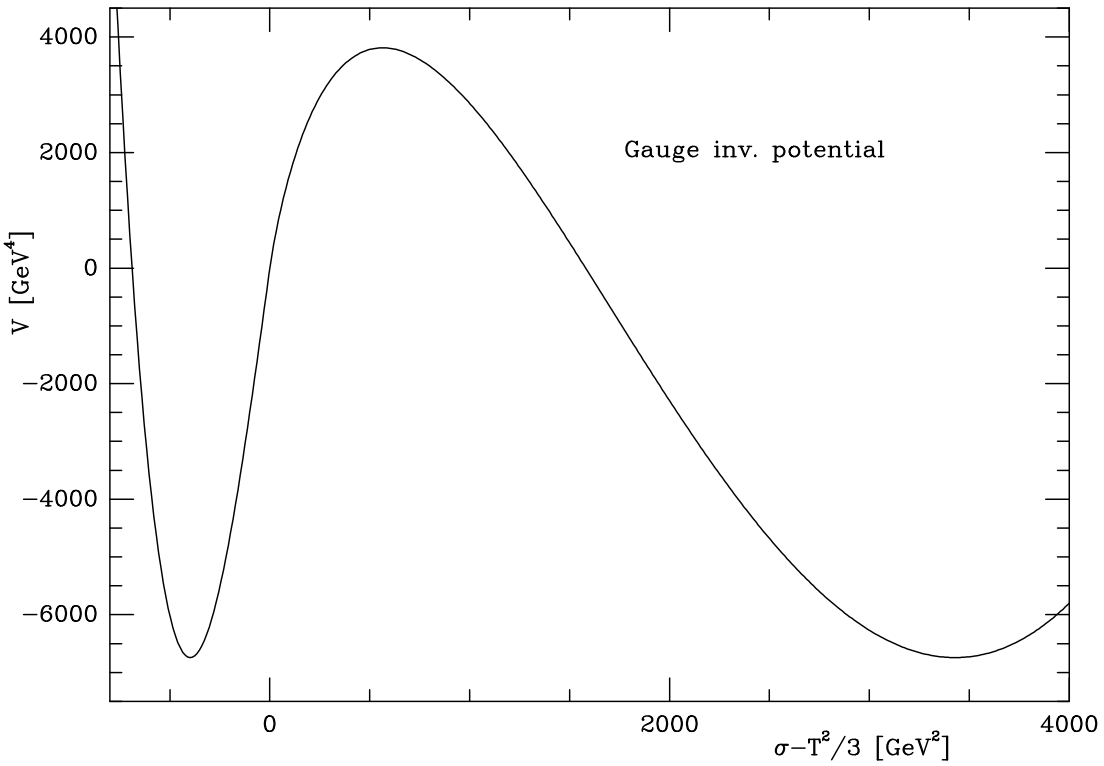

Fig.4.1 Gauge invariant effective potential at critical temperature, m_{Higgs}=70GeV

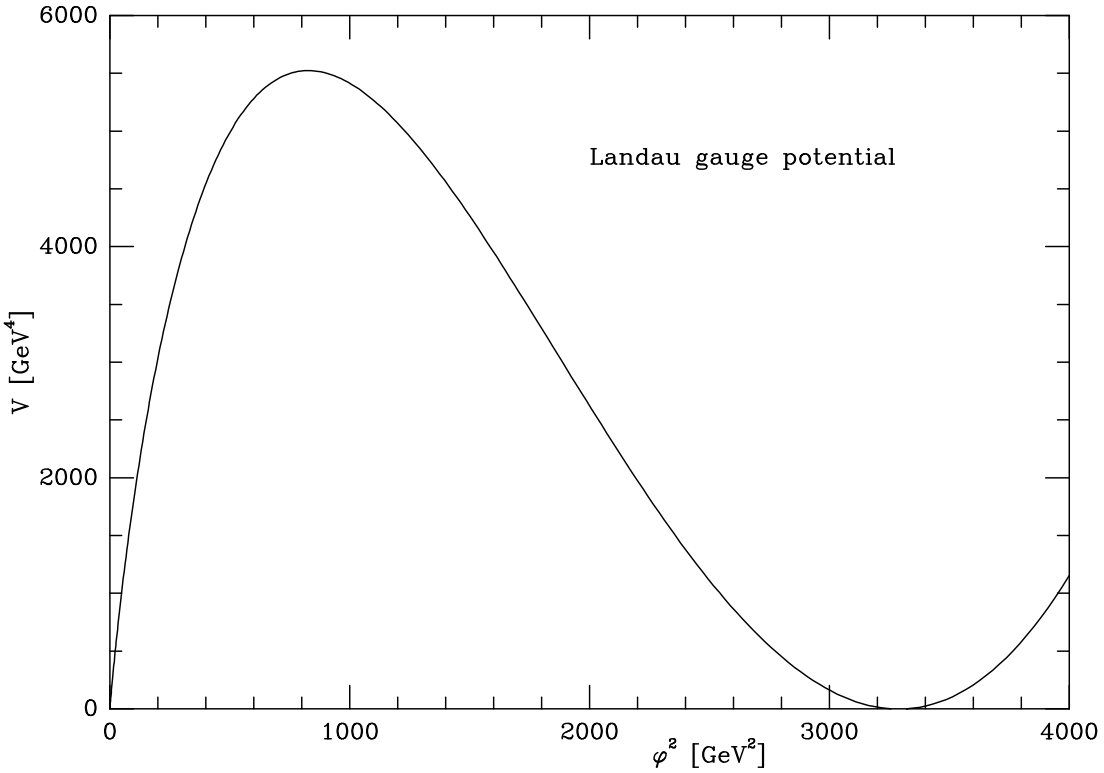

Fig.4.2 Effective potential in Landau gauge at critical temperature, m_{Higgs}=70 GeV

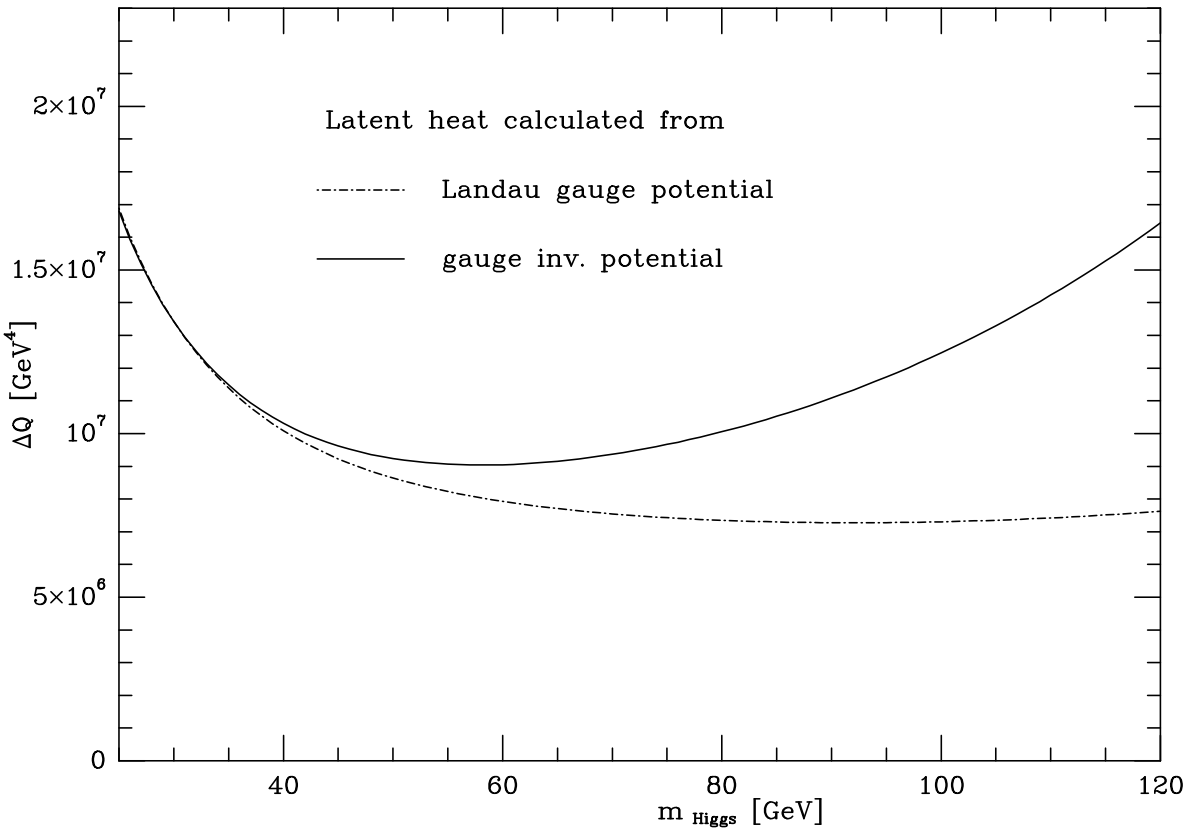

Fig.4.3 Latent heat as a function of the zero temperature Higgs mass, calculated from the potential in Landau gauge and from the gauge invariant potential

The main difference of the gauge invariant and the Landau gauge potential lies in the description of the symmetric phase. Choosing the expectation value of the basic field operator as order parameter the symmetric phase corresponds to exactly one point, where this parameter must vanish. In contrast to this, the gauge invariant coupling of the source permits a description of the symmetric phase by a non-trivial minimum of the free energy as a function of the field square expectation value. This expectation value can be made smaller than its value at the minimum by turning the source, i.e. the mass term, on. Therefore the gauge invariant potential exhibits a very steep behaviour left from the symmetric minimum, but no definite smallest value of σ'.

Note, that the gauge invariant potential is continuous together with its first derivative at the matching point $\sigma' = 0$. This is due to the difference of the first terms of eqs. (4.19) and (4.20) which compensates the contribution of the last term of eq. (4.19) to the derivative at $\sigma' = 0$. The additional resummation up to order g^3 performed in section 4.1 is responsible for that matching. However, the same result for $V(\sigma)$ can also be obtained with leading

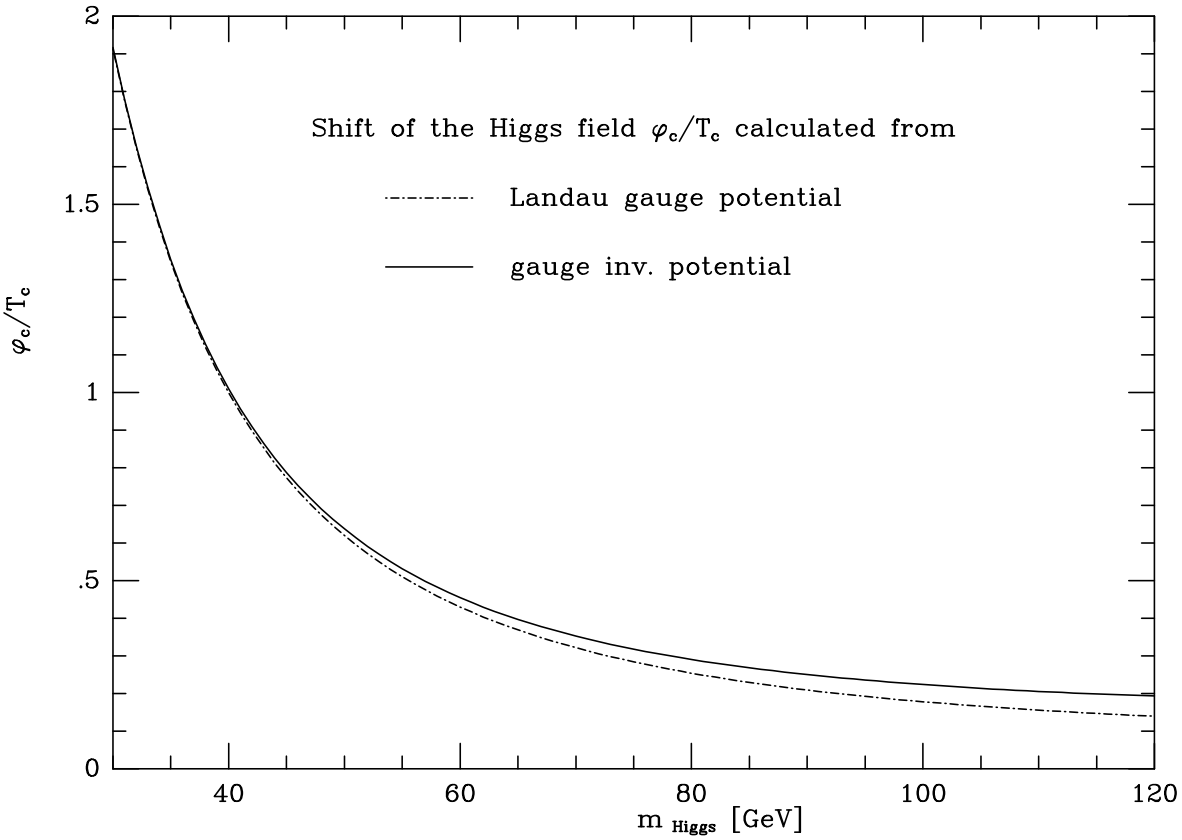

Fig.4.4 Shift of the Higgs field as a function of the Higgs mass, calculated from the potential in Landau gauge and from the gauge invariant potential

order resummation only. In that case the contribution

$$\frac{3g^2T^2}{32\pi^2}Mm_{L,0} = \frac{1}{2}\alpha_{02}T^2\sigma' \tag{4.21}$$

from the scalar-vector diagram of the type of fig. 1.2.b appears in the symmetric phase, thus rescuing the above matching of the first derivatives.

At small Higgs masses the symmetric minimum of the gauge invariant potential is not important numerically. Therefore in this region the form of the potential at the critical temperature and the derived phase transition parameters are very close to the Landau gauge results. However, already at $m_{\rm Higgs} = 70$ GeV the symmetric minimum leads to an increase of the barrier height by a factor of ≈ 2 (compare figs. 4.1 and 4.2). This effect becomes even more important for larger Higgs masses. The latent heat plotted in fig. 4.3 does also show a stronger first order phase transition at large Higgs mass values suggested by the new approach. Note that a similar behaviour of the latent heat as a function of the Higgs mass has been obtained from the two-loop results in Landau gauge (see fig. 3.4). The jump of the order parameter shown in fig. 4.4 is not seriously affected by the new approach. This

justifies the conjecture of section 3.3.1 that this parameter is reliably determined by the Landau gauge calculation.

Due to the separate treatment of the symmetric and the broken phase in the gauge invariant approach, it is not clear at present how the surface tension can be calculated. However, due to the strong increase of the barrier height at large Higgs masses in the new approach significant changes with respect to the Landau gauge results are expected.

4.3 Problems at higher orders

It is, in principle, straightforward to extend the calculation of the previous sections to the order g^4, λ^2, as it has been done in the conventional Landau gauge calculation of chapters 2 and 3. Nevertheless, the concrete realization of this project is hampered by some problems to be discussed in the sequel.

The first step is to supply the leading order results for $W(J)$, given by eqs. (4.13) and (4.14), with higher order corrections. It is advantageous to calculate in Landau gauge, although of course the final result should be gauge independent by definition. The necessary corrections include the next term of the high temperature expansion of the one-loop integrals and the leading contributions of the two-loop graphs. The later ones, which form the main part of the calculation, can be obtained using the formulae of appendix B.3 and changing the masses appropriately. Note that in the broken phase, one-particle reducible two-loop graphs have to be considered.

To make $W(J)$ finite, the parameters of the Lagrangian are renormalized multiplicatively in the conventional way, using e.g. the SU(2)-limit of eqs. (B.20). Note that the multiplicative mass renormalization has to be applied to both $-\nu$ and J. However, a finite result is obtained only after the additional counterterm

$$W_{c.t.} = \frac{1}{16\pi^2\epsilon}(J-\nu)^2 \tag{4.22}$$

has been added to $W(J)$ in both the symmetric and the broken phase calculation (compare ref. [55]). It is claimed that a possible finite part of this counterterm, common to both phases, does not affect the physical parameters derived from the calculation. Firstly, constant and linear term in J do only shift the Legendre transformed function along vertical and horizontal axis respectively. Applying such a shift to both phases does not change the description of the phase transition. Secondly, the quadratic term in J does not affect the minimum of the Legendre transformed function, since at the minimum $J = 0$ and the quadratic correction

vanishes together with its first derivative [53]. To see this more explicitly introduce the corrected function $\tilde{W}(J)$, defined by

$$\tilde{W}(J) = W(J) + CJ^2. \tag{4.23}$$

The new position of the minimum of the potential is given by

$$\frac{\tilde{\sigma}_{min}}{2} = \left.\frac{\partial \tilde{W}}{\partial J}\right|_{J=0} = \left.\frac{\partial W}{\partial J}\right|_{J=0} = \frac{\sigma_{min}}{2}\,, \tag{4.24}$$

and analogously

$$\tilde{V}_{min} = \tilde{W}(0) = W(0) = V_{min}\,. \tag{4.25}$$

Performing the Legendre transformation perturbatively a higher order dependence of the result on the finite part of $W_{c.t.}$ is nevertheless present.

Now the obvious way to proceed is to calculate $V(\sigma)$ using eq. (4.16). In the broken phase W_2 is given by the order g^4, λ^2 corrections and the first three terms of the perturbative expansion of V can be calculated. In the symmetric phase, where no tree-level term exists, these two-loop corrections define W_1 and only the first two terms of eq. (4.16) are to be used.

It has been checked that the complete potential is continuous at the matching point $\sigma' = 0$. However, its first derivative is logarithmically divergent at this point. Since all physical information is extracted from the minima of the potential this pathology should, in principle, have no importance.

The convincing form of the potential illustrated in fig. 4.1 has been obtained due to the additional resummation of the scalar mass. More precisely, the scalar mass has been resummed to the same order to which the whole calculation was performed. Therefore it appears necessary to extend the resummation to the order g^4, λ^2 in this section. Unfortunately, this can not be done in a straightforward manner, because the two-loop scalar self-energy is divergent at zero momentum. Another possible way to organize the higher order resummation would be to demand the continuity of the first derivative of the potential. This fails due to the same infrared divergences. However, it has been seen numerically that such a higher order resummation can change the physical picture of the phase transition significantly.

It is not known at present, how the above problems, which are essentially connected with the infrared divergences of a massless three-dimensional field theory, can be resolved.

4.4 On the relation to the conventional effective potential

The gauge invariant thermodynamic potential $W(J)$, introduced in the beginning of this chapter, has a simple relation to the effective potential, as it can be calculated in any fixed gauge [56]:

$$\begin{aligned}
\exp(-\beta\Omega W) &= \int D\Phi D\Phi^\dagger DW_\mu \exp\left[\int_\beta dx(\mathcal{L} - J\Phi^\dagger\Phi)\right] \qquad (4.26)\\
&= 2\pi^2 \int \varphi^3 d\varphi \int D\Phi D\Phi^\dagger DW_\mu\, \delta\left(\varphi - \frac{1}{\beta\Omega}\int_\beta dx\, \varphi_1(x)\right)\\
&\qquad \prod_{i=2}^{4} \delta\left(\frac{1}{\beta\Omega}\int_\beta dx\, \varphi_i(x)\right) \exp\left[\int_\beta dx(\mathcal{L} - J\Phi^\dagger\Phi)\right]\\
&= 2\pi^2 \int \varphi^3 d\varphi \exp\left[-\beta\Omega V(\varphi, J)\right] .
\end{aligned}$$

Here φ_i are the real components of Φ (see eq. (3.3)) and $V(\varphi, J)$ is the Landau gauge effective potential of a theory with mass square $-\nu + J$. In the infinite volume limit only the absolute minimum φ_{min} of V contributes to the φ-integral in eq. (4.26), resulting in the relation

$$W(J) = V(\varphi_{min}, J)\,. \qquad (4.27)$$

The thermodynamic potential $W(J)$, calculated by this method, is continuous, but its first derivative has a discontinuity at the critical temperature and $J = 0$, generated by the jump of the absolute minimum φ_{min} from zero to the non-trivial, symmetry-breaking minimum φ_+. This discontinuity corresponds to the shift of the field square expectation value σ

$$-\frac{1}{2}\Delta\sigma = \left.\frac{\partial W}{\partial J}\right|_{J=0_-} - \left.\frac{\partial W}{\partial J}\right|_{J=0_+} = \frac{\partial}{\partial J}\Big[\, V(\varphi_+, J) - V(0, J)\Big]\,. \qquad (4.28)$$

Considering only the leading terms of the Landau gauge potential V, the approximate result is

$$-\frac{1}{2}\Delta\sigma = \frac{\partial}{\partial J}\Big[\,\frac{1}{2}(-\nu + J + \alpha_{01}T^2)\varphi_+^2 + \cdots\Big] \approx \frac{1}{2}\varphi_+^2\,. \qquad (4.29)$$

This relation justifies the way in which the Landau gauge and the gauge invariant calculations have been compared in section 4.2, in particular in figures 4.1, 4.2 and 4.4.

The conventional definition of the latent heat from $W(J)$ gives immediately, via eq. (4.27), the formula used in the Landau gauge investigation (eq. 2.22)).

Note however, that the gauge invariant $W(J)$ has been calculated in a completely different manner in section 4.1. There, it has only played an intermediate role in the calculation

of $V(\sigma)$. The approach was based on the identification of the minimum of the tree-level potential and a subsequent loop expansion around this minimum.

In contrast to the paragraph above, a different approach has been taken in this section. After shifting the scalar field, the effective potential $V(\varphi, J)$ which includes loop corrections, is determined. Its minimum then gives the thermodynamic potential $W(J)$.

The way in which the scalar masses have been resummed in the Landau gauge calculations of chapters 2 and 3 is not unique. If only the minima of the potential are to be considered, as suggested by eq. (4.27), it may be advantageous to resum differently in the symmetric and in the broken phase. In particular such a method can take into account the fact that the Goldstone boson mass has to be zero at the broken minimum. One-loop calculations, based on this idea, reproduce the numerical results of section 4.2 exactly. A corresponding two-loop investigation is under way [22].

The above method, based on the derivatives of $W(J,T)$ near its non-analytic point, has its disadvantage. No information can be extracted concerning the metastable and unstable states, thus disabling the usual derivative expansion approach to the surface tension.

4.5 Clausius-Clapeyron equation

In classical thermodynamics there is a well known relation between the latent heat of a phase transition and the change of the molar volume, the Clausius-Clapeyron equation [57]. In complete analogy a relation between latent heat and jump of the order parameter σ can be written down.

Describing the state of the system by the gauge invariantly coupled source J and the temperature the phase transition curve is given by a function $J_{crit.}(T)$. Since $W(J,T)$ is continuous in the J-T-plane, the total derivative of W along the phase curve

$$\frac{dW}{dT} = \frac{\partial W}{\partial J}\,\frac{dJ_{crit.}}{dT} + \frac{\partial W}{\partial T} \tag{4.30}$$

is equal in both phases. The partial derivatives of W can be easily related to the field square expectation value σ and the energy density E:

$$\frac{\partial W}{\partial J} = \frac{1}{2}\sigma \qquad , \qquad \frac{\partial W}{\partial T} = \frac{1}{T}(W - E)\,. \tag{4.31}$$

Now, evaluating eq. (4.30) in both phases and equating the results gives

$$\frac{1}{2}\Delta\sigma\frac{dJ_{crit.}}{dT} = \frac{\Delta Q}{T}\,, \tag{4.32}$$

where $\Delta Q = E_{symmetric} - E_{broken}$ is the latent heat.

Neglecting effects of higher loops und renormalization $dJ_{crit.}/dT$ can be easily evaluated by dimensional arguments. Since the Higgs mass term $-\nu + J$ is the only dimensionful parameter of the SU(2)-Higgs model the dependence of the critical temperature on J is given by

$$T = \text{const.}\sqrt{\nu - J_{crit.}}\,. \tag{4.33}$$

From this

$$T\frac{dJ_{crit.}}{dT}\bigg|_{J=0} = -2\nu \tag{4.34}$$

and therefore the jump of the order parameter and the latent heat are related by

$$\Delta Q = -\frac{1}{2}m^2_{\text{Higgs}}\Delta\sigma\,, \tag{4.35}$$

where m_{Higgs} is the zero temperature Higgs mass.

This relation has been checked against the available data from one- and two-loop calculations of the effective potential. The Landau gauge results are in very good agreement with eq. (4.35) at small Higgs masses, with deviations increasing up to $\sim 25\%$ at m_{Higgs}=80 GeV. It is interesting to observe that the gauge invariant one-loop calculation of section 4.2 satisfies the above relation exactly. This can be proven analytically, by writing the gauge invariant potential in the form

$$V(\sigma) = -\frac{\nu}{2}\sigma + T^4\tilde{V}(\sigma/T^2) \tag{4.36}$$

with some dimensionless function $\tilde{V}$, which has no implicit temperature dependence. From this general form of V and the definitions of $\Delta\sigma$ and ΔQ the relation (4.35) can be easily extracted.

Note also, that the lattice results of ref. [12] verify eq. (4.35) quite well. For L_t=3 lattices the deviation amounts to no more than 1...2 standard deviations, defined by the statistical error of the simulation. Here L_t denotes the lattice size in time like direction. An improvement of the validity of eq. (4.35) is observed when going from $L_t = 2$ to $L_t = 3$ lattices.

Conclusions

The thermodynamic parameters of the electroweak phase transition have been analysed in a perturbative approach based on the high temperature effective potential. A complete calculation of the g^4, λ^2-potential has been performed for the Abelian Higgs model, the SU(2)-Higgs model and the standard model. The Abelian calculation has been shown to have no infrared problems in the systematic coupling constant expansion in the symmetric phase. This does not hold in the general case, where the typical non-Abelian diagrams become important in higher orders. This is seen explicitly at the order g^4, where, opposite to the Abelian case, logarithmic mass terms increase the strength of the first order phase transition dramatically.

Critical temperature, latent heat, surface tension and jump of the order parameter $\Phi^\dagger\Phi$ have been calculated for different Higgs masses and different approximations to the potential. The reliability of the perturbative expansion is clearly worsening with increasing Higgs mass. In particular, in the non-Abelian case, any information on an infrared cutoff, e.g. a magnetic mass value, would increase the accuracy of the calculation drastically. However, infrared problems are also connected with scalar masses, which become small at the critical temperature.

Comparing the complete standard model with the pure SU(2)-Higgs model no qualitative change is found. The main difference is a decrease of the strength of the phase transition due to the large top quark mass.

Newly available lattice data at $m_{\text{Higgs}} \approx 18$ GeV and at $m_{\text{Higgs}} \approx 49$ GeV [11, 12] are in good quantitative agreement with the perturbative two-loop results. This may be seen as a justification to take the calculated parameters more seriously at larger Higgs mass values, where convergence of the perturbation series is bad and no lattice data is available. Perturbative results suggest a weak first order phase transition at realistic Higgs mass values. However, a change to an analytic crossover is also a possibility [50]. Unfortunately, the region where reliable predictions are available and where $\varphi \sim T$, an important condition for

baryogenesis, is at $m_{\rm Higgs} \approx 40$ GeV and therefore well below the experimental bound. The present results seem to disfavour scenarios of electroweak baryogenesis relying on a strong first order phase transition within the minimal standard model.

The gauge invariant description, elaborated in the last chapter, allows a better physical understanding of the thermodynamics of the phase transition. In this approach, coupling the source term in a gauge invariant manner, a more direct access to physical quantities is possible. In particular, the symmetric phase is described by a non-trivial minimum of the potential as well. Since the numerical results obtained in the gauge invariant approach at one-loop are similar to the Landau gauge results, the latter ones are strongly supported by the new, conceptually more satisfactory treatment. Applying the Clausius-Clapeyron equation to the electroweak phase transition a simple relation between latent heat and jump of the order parameter has been derived in the above context. Being in good agreement with perturbative as well as with lattice data, it improves confidence in the correctness of the treatment of the phase transition.

In agreement with recent results of other methods the performed investigation predicts a first order electroweak phase transition of decreasing strength when the Higgs mass is increasing up to $m_{\rm Higgs} \approx 70$ GeV. At larger Higgs mass values the calculation is strongly affected by infrared problems. If, in spite of this difficulty, perturbation theory without explicit infrared cutoff is taken seriously, the phase transition is found to remain weakly first order.

Acknowledgements

I am most grateful to my advisor, Prof. W. Buchmüller, who suggested this investigation, for continuous support and encouragement. During the intensive and fruitful collaboration, I had many invaluable opportunities to learn from him. I would like to thank Dr. Z. Fodor, with whom I collaborated during large parts of this investigation, for sharing his ideas with me, for many highly instructive discussions and, in particular, for patiently explaining the lattice results to me. At different stages of the work presented in this thesis, I profited from discussions with Dr. D. Bödeker, J. Hein, Dr. T. Helbig, Dr. B. Kniehl, Dr. H.-G. Kohrs and Dr. O. Philipsen. I thank them for their interest in my work. Finally, I would like to thank all my colleagues and friends at DESY for the enjoyable working atmosphere.

Appendix A

Some integrals

A.1 Integrals of thermal field theory

In this section the basic temperature integrals [17, 34, 42, 58], needed throughout the calculation, are listed. The notation follows the general formalism introduced in section 1.1. At one-loop level, the fundamental integral is [17, 42]

$$\begin{aligned} I(m) &= \sum\!\!\!\!\!\!\int \frac{dk}{k^2+m^2} = \frac{\mu^{2\epsilon}}{(2\pi)^{n-1}\beta}\sum_{k_0}\int d^{n-1}k \frac{1}{k^2+m^2} \\ &= \frac{1}{12\beta^2}(1+\epsilon\iota_\epsilon) - \frac{m}{4\pi\beta} - \frac{m^2}{16\pi^2}\left(\frac{1}{\epsilon}+\ln\bar{\mu}^2\beta^2+\frac{3}{2}-c_1\right)+\dots\,, \end{aligned} \tag{A.1}$$

where

$$c_1 = \tfrac{3}{2} + 2\ln 4\pi - 2\gamma_E \approx 5.4076\,. \tag{A.2}$$

Here terms of higher order in $m\beta$ have been neglected because in the present calculation they do not contribute to the g^4-potential. The renormalization scale of the $\overline{\rm MS}$-formalism is defined by

$$\ln\bar{\mu}^2 = \ln\mu^2 + \ln 4\pi - \gamma_E\,, \tag{A.3}$$

where γ_E is Euler's constant. The coefficient

$$\iota_\epsilon = 2\gamma_E + \ln\frac{\bar{\mu}^2\beta^2}{4} - \frac{12}{\pi^2}\zeta'(2) \tag{A.4}$$

of ϵ from the leading contribution

$$I^\epsilon_\beta = \frac{1}{12\beta^2}(1+\epsilon\iota_\epsilon) \tag{A.5}$$

will cancel in the final formula for the potential, similarly to the temperature dependent divergences [17].

The fermionic analogue of this integral is

$$\begin{aligned} I_f(m) &= \sum\!\!\!\!\!\!\int_f \frac{dk}{k^2+m^2} \\ &= -\frac{1}{24\beta^2}\left(1+\epsilon(\iota_\epsilon - \ln 4)\right) - \frac{m^2}{16\pi^2}\left(\frac{1}{\epsilon} + \ln\bar{\mu}^2\beta^2 + \frac{3}{2} - c_1 + 2\ln 4\right) . \end{aligned} \tag{A.6}$$

Its leading, mass independent, part will be denoted by $I^\epsilon_{f\beta}$.

Another bosonic one-loop integral, appearing due to the non-covariant structure of the vector propagator, is given by

$$I\!I(m) = \sum\!\!\!\!\!\!\int \frac{k_0^2\,dk}{k^2(k^2+m^2)} = \left(-\frac{1}{2}+\epsilon\right) I^\epsilon_\beta - \frac{m^2}{64\pi^2}\left(\frac{1}{\epsilon} + \ln\bar{\mu}^2\beta^2 + \frac{7}{2} - c_1\right) . \tag{A.7}$$

At two-loop level the basic problem is the calculation of the scalar setting sun diagram (see fig. 1.2.a). This has first been done in ref. [34] and extended to the case of three different masses in ref. [17]. Neglecting terms of order $m^2\beta^2$ the integral reads

$$\begin{aligned} H(m_1,m_2,m_3) &= \sum\!\!\!\!\!\!\int\!\!\sum\!\!\!\!\!\!\int \frac{dk\,dq}{(k^2+m_1^2)(q^2+m_2^2)((k+q)^2+m_3^2)} \\ &= \frac{3}{16\pi^2\epsilon} I^\epsilon_\beta + \frac{1}{64\pi^2\beta^2}\left(\ln\bar{\mu}^2\beta^2 - 4\ln\frac{\beta(m_1+m_2+m_3)}{3} - c_2\right) , \end{aligned} \tag{A.8}$$

where the constant

$$c_2 = 2\left(\gamma_E - \frac{\zeta'(2)}{\zeta(2)} + \ln\frac{9}{2} - 1\right) \approx 3.3025 \tag{A.9}$$

has first been obtained analytically in ref. [58].

In the standard model calculation the fermionic analogue of this two-loop integral, i.e. the corresponding integral where two of the propagators have fermionic Matsubara frequencies $k_0 = (2n+1)\pi T$, is needed. However, as has been shown in ref. [17], this integral vanishes in leading order in dimensional regularization when $\epsilon \to 0$:

$$\sum\!\!\!\!\!\!\int_f\!\!\sum\!\!\!\!\!\!\int \frac{dk\,dq}{(k^2+m_1^2)(q^2+m_2^2)((k+q)^2+m_3^2)} = \frac{1}{\beta^2}O(m^2\beta^2). \tag{A.10}$$

A.2 One- and two-point functions

For the convenience of the reader the usual one- and two-point functions, necessary for the renormalization at $T=0$, are displayed. Working in $n = 4-2\epsilon$ dimensions only the pole and the finite parts are shown.

$$A(m^2) = \frac{\mu^{2\epsilon}}{(2\pi)^n}\int \frac{d^nk}{k^2-m^2+i\varepsilon} = \frac{im^2}{16\pi^2}\left(\frac{1}{\epsilon}+1+\ln\frac{\bar{\mu}^2}{m^2}\right) , \tag{A.11}$$

$$
\begin{aligned}
B(q^2, m_0^2, m_1^2) &= \frac{\mu^{2\epsilon}}{(2\pi)^n} \int \frac{d^n k}{(k^2 - m_0^2 + i\varepsilon)((k+q)^2 - m_1^2 + i\varepsilon)} \qquad \text{(A.12)} \\
&= \frac{i}{16\pi^2} \left[\frac{1}{\epsilon} + 2 + \ln \frac{\bar{\mu}^2}{m_0 m_1} - \frac{1}{q^2} \left\{ (m_1^2 - m_0^2) \ln \frac{m_1}{m_0} - 2 m_1 m_0 f(x) \right\} \right] ,
\end{aligned}
$$

where

$$
x = \frac{m_0^2 + m_1^2 - q^2}{2 m_0 m_1} \qquad \text{(A.13)}
$$

and the function f is defined by

$$
f(x) = \begin{cases}
\sqrt{x^2 - 1}\,(-\operatorname{arccosh}(-x) + i\pi) & : \quad x < -1 \\
-\sqrt{1 - x^2}\,\arccos x & : \quad -1 < x < 1 \\
\sqrt{x^2 - 1}\,\operatorname{arccosh} x & : \quad 1 < x \quad .
\end{cases} \qquad \text{(A.14)}
$$

Appendix B

Explicit formulae for the effective potential

B.1 Abelian Higgs model

The leading order resummed masses of Goldstone boson, Higgs particle and longitudinal vector boson read

$$\begin{aligned} m_\chi^2 &= \lambda\varphi^2 - \nu + (4\lambda + (3-2\epsilon)e^2)I_\beta^\epsilon &= \lambda\varphi^2 - \nu + \frac{4\lambda+3e^2}{12\beta^2} + O(\epsilon)\,, \\ m_\varphi^2 &= m_\chi^2 + 2\lambda\varphi^2\,, \\ m_L^2 &= e^2\varphi^2 + 4e^2(1-\epsilon)I_\beta^\epsilon &= e^2\varphi^2 + \frac{e^2}{3\beta^2} + O(\epsilon)\,. \end{aligned} \tag{B.1}$$

The transverse vector mass $m_T = m = e\varphi$ remains uncorrected. For the calculation of V_R the self-energy parts of the type Π_{b2} (see eq. (1.20)) are needed. They appear only for the longitudinal and transverse vector boson:

$$\Pi_{b2,L} = (2-4\epsilon)e^2 I_\beta^\epsilon \quad , \quad \Pi_{b2,T} = -2e^2 I_\beta^\epsilon\,. \tag{B.2}$$

The counterterms rendering the potential finite are generated from the leading order contribution (see the first two terms of eq. (B.7) below):

$$\begin{aligned} \delta V &= \frac{\varphi^2}{2}\Big[-\nu(\delta Z_\nu + \delta Z_{\varphi^2}) + I_\beta^\epsilon \left\{ 4\lambda(\delta Z_\lambda + \delta Z_{\varphi^2}) + (3-2\epsilon)e^2(\delta Z_{e^2} + \delta Z_{\varphi^2}) \right\} \Big] \\ &\quad + \frac{\lambda}{4}\varphi^4(\delta Z_\lambda + 2\delta Z_{\varphi^2})\,, \end{aligned} \tag{B.3}$$

where

$$\delta Z_\lambda = \left(\frac{3e^4}{\lambda} - 6e^2 + 10\lambda \right) p\,, \quad \delta Z_{e^2} = \frac{e^2}{3}p\,, \quad \delta Z_\nu = (4\lambda - 3e^2)p\,, \quad \delta Z_{\varphi^2} = 3e^2 p\,, \tag{B.4}$$

with the pole in ϵ denoted by

$$p = \frac{1}{16\pi^2\epsilon}. \tag{B.5}$$

The different contributions to the potential, listed below, have to be summed according to eq. (1.30), where

$$V_\ominus = V_a + V_b + V_p \tag{B.6}$$

is given by the diagrams in fig. 2.1. Linear mass terms, poles in ϵ and terms proportional to ι_ϵ (see eq. (A.4)), which cancel systematically in the final result, are not shown and the limit $\epsilon \to 0$ has already been performed. A finite contribution from δV has been added to V_4. The following terms form the complete analytic $\overline{\text{MS}}$-potential:

$$V_3 = \frac{\varphi^2}{2}\left[-\nu + \frac{1}{\beta^2}\left(\frac{1}{3}\lambda + \frac{1}{4}e^2\right)\right] + \frac{\lambda}{4}\varphi^4 - \frac{1}{12\pi\beta}\left[m_\varphi^3 + m_\chi^3 + 2m^3 + m_L^3\right] \tag{B.7}$$

$$\begin{aligned} V_a = \frac{e^2}{32\pi^2\beta^2}\Bigg[& m^2\left(\ln\frac{\beta}{3} - \frac{1}{12}\ln\bar{\mu}^2\beta^2 - \frac{1}{6}c_1 + \frac{1}{4}c_2 + \frac{1}{4}\right) - m(m_\varphi + m_\chi) \\ & + m_\varphi m_\chi + \frac{1}{2}(m_\varphi^2 + m_\chi^2)(-4\ln\frac{\beta}{3} + \ln\bar{\mu}^2\beta^2 - c_2) - \frac{1}{m^2}(m_\varphi^2 - m_\chi^2)^2\ln(m_\varphi + m_\chi) \\ & - \frac{1}{m}(m_\varphi - m_\chi)^2(m_\varphi + m_\chi) + \frac{1}{m^2}\left\{m^4 - 2(m_\varphi^2 + m_\chi^2)m^2 + (m_\varphi^2 - m_\chi^2)^2\right\}\ln(m_\varphi + m_\chi + m)\Bigg] \end{aligned} \tag{B.8}$$

$$\begin{aligned} V_b = \frac{e^2}{64\pi^2\beta^2}\Bigg[& 5m^2\left(\frac{1}{2}c_2 - \ln\frac{9\bar{\mu}}{\beta}\right) + \left(8m^2 - 4m_\varphi^2 + \frac{m_\varphi^4}{m^2}\right)\ln(2m + m_\varphi) \\ & - \frac{2}{m^2}(m^2 - m_\varphi^2)^2\ln(m + m_\varphi) + 4m^2\ln(2m_L + m_\varphi) + \frac{m_\varphi^4}{m^2}\ln m_\varphi + 2mm_\varphi + m_\varphi^2\Bigg] \end{aligned} \tag{B.9}$$

$$V_p = -\frac{\lambda^2\varphi^2}{16\pi^2\beta^2}\left[\ln\frac{3\mu^2}{\beta^2} - c_2 - \ln\{m_\varphi^3(m_\varphi + 2m_\chi)\}\right] \tag{B.10}$$

$$V_4 = \frac{e^2\varphi^2}{64\pi^2\beta^2}\left[\frac{4}{3}\lambda - e^2\left(\frac{35}{18} + \ln\bar{\mu}^2\beta^2 - c_1\right)\right] \tag{B.11}$$

$$-\frac{1}{64\pi^2}\left\{\left(m_\varphi^4+m_\chi^4+3m^4\right)\left(\ln\bar{\mu}^2\beta^2+\frac{3}{2}-c_1\right)-2m^4\right\}$$

$$V_z=\frac{1}{32\pi^2\beta^2}\left[\frac{3}{2}\lambda(m_\varphi^2+m_\chi^2)+\lambda m_\varphi m_\chi+e^2(m_L+2m)(m_\varphi+m_\chi)\right] \tag{B.12}$$

B.2 Standard model

The leading order resummed masses of Goldstone boson and Higgs particle read

$$\begin{aligned} m_2^2 &= \lambda\varphi^2-\nu+\left(6\lambda+\frac{3g_2^2+g_1^2}{4}(3-2\epsilon)\right)I_\beta^\epsilon-6g_Y^2I_{f\beta}^\epsilon \\ &= \lambda\varphi^2-\nu+\frac{1}{12\beta^2}\left(6\lambda+\frac{9}{4}g_2^2+\frac{3}{4}g_1^2+3g_Y^2\right)+O(\epsilon)\ , \\ m_1^2 &= m_2^2+2\lambda\varphi^2\ . \end{aligned} \tag{B.13}$$

While the transverse vector boson masses and the fermion mass remain uncorrected to leading order

$$m_W=\frac{1}{2}g_2\varphi\quad,\quad m_Z=m_W/\cos\theta_W\quad,\quad m_f=\frac{1}{\sqrt{2}}g_Y\varphi\,, \tag{B.14}$$

the longitudinal SU(2)×U(1) mass matrix receives temperature corrections in the diagonal elements [15]

$$\begin{aligned} \delta m_{WL}^2 &= g_2^2\left[(10-18\epsilon)I_\beta^\epsilon-8n_f(1-\epsilon)I_{f\beta}^\epsilon\right] = \frac{g_2^2}{\beta^2}\left(\frac{5}{6}+\frac{1}{3}n_f\right)+O(\epsilon)\ , \\ \delta m_{BL}^2 &= g_1^2\left[(2-2\epsilon)I_\beta^\epsilon-\frac{40}{3}n_f(1-\epsilon)I_{f\beta}^\epsilon\right] = \frac{g_1^2}{\beta^2}\left(\frac{1}{6}+\frac{5}{9}n_f\right)+O(\epsilon)\ . \end{aligned} \tag{B.15}$$

They result in longitudinal masses defined by

$$\begin{pmatrix} m_W^2+\delta m_{WL}^2 & -\frac{1}{4}g_1g_2\varphi^2 \\ -\frac{1}{4}g_1g_2\varphi^2 & m_B^2+\delta m_{BL}^2 \end{pmatrix}=\begin{pmatrix} \cos\tilde{\theta} & \sin\tilde{\theta} \\ -\sin\tilde{\theta} & \cos\tilde{\theta} \end{pmatrix}\begin{pmatrix} m_{ZL}^2 & 0 \\ 0 & m_{\gamma L}^2 \end{pmatrix}\begin{pmatrix} \cos\tilde{\theta} & -\sin\tilde{\theta} \\ \sin\tilde{\theta} & \cos\tilde{\theta} \end{pmatrix}. \tag{B.16}$$

In the following the short hand notations

$$s=\sin\theta_W\quad,\quad c=\cos\theta_W\quad,\quad \tilde{s}=\sin\tilde{\theta}\quad,\quad \tilde{c}=\cos\tilde{\theta} \tag{B.17}$$

are used. From eq. (B.16) several helpful identities can be derived:

$$\begin{aligned} m_{ZL}^2 m_{\gamma L}^2 &= m_Z^2 \left[c^2 \delta m_{BL}^2 + s^2 \delta m_{WL}^2\right] + \delta m_{BL}^2 \delta m_{WL}^2 \\ m_{ZL}^2 + m_{\gamma L}^2 &= m_Z^2 + \delta m_{WL}^2 + \delta m_{BL}^2 \\ m_{ZL}^4 + m_{\gamma L}^4 &= \left[m_Z^2 + \delta m_{WL}^2 + \delta m_{BL}^2\right]^2 - 2 m_Z^2 \left[c^2 \delta m_{BL}^2 + s^2 \delta m_{WL}^2\right] . \end{aligned} \tag{B.18}$$

For the calculation of V_R self-energy parts of the type $\Pi_{a2}(k)$ and Π_{b2} are needed:

$$\begin{aligned} \Pi_{b2}^{scalars} &= -6 g_Y^2 I_{f\beta}^{\epsilon} \quad , \quad \Pi_{a2,L}^{WW}(k) = 2 g^2 I_{\beta}^{\epsilon}(1-\epsilon)\frac{k_0^2}{k^2} , \\ \Pi_{b2,T}^{WW} &= -g_2^2(6-4\epsilon) I_{\beta}^{\epsilon} \quad , \quad \Pi_{b2,L}^{WW} = g_2^2 \left[2(3-8\epsilon) I_{\epsilon}^{\beta} - 8 n_f (1-\epsilon) I_{f\beta}^{\epsilon}\right] \cdot \\ \Pi_{b2,T}^{BB} &= -g_1^2 I_{\beta}^{\epsilon} \quad , \quad \Pi_{b2,L}^{BB} = g_1^2 \left[(1-2\epsilon) I_{\epsilon}^{\beta} - \frac{40}{3} n_f (1-\epsilon) I_{f\beta}^{\epsilon}\right] \end{aligned} \tag{B.19}$$

In complete analogy with the Abelian case (see eq. (B.3)) the counterterms are generated from the leading order potential given by the first line of eq. (B.21). The multiplicative renormalization realizing the $\overline{\rm MS}$-scheme is described by

$$\delta Z_{\varphi^2} = \left(\frac{9}{4} g_2^2 + \frac{3}{4} g_1^2 - 3 g_Y^2\right) p , \quad \delta Z_{g_1^2} = g_1^2 \left(\frac{1}{6} + \frac{20}{9} n_f\right) p , \quad \delta Z_{g_2^2} = g_2^2 \left(-\frac{43}{6} + \frac{4}{3} n_f\right) p ,$$

$$\delta Z_{\lambda} = \frac{1}{\lambda} \left(-3 g_Y^4 + \frac{3}{16} g_1^4 + \frac{3}{8} g_1^2 g_2^2 + \frac{9}{16} g_2^4 + 6 \lambda g_Y^2 - \frac{3}{2} \lambda g_1^2 - \frac{9}{2} \lambda g_2^2 + 12 \lambda^2\right) p , \tag{B.20}$$

$$\delta Z_{g_Y} = \left(\frac{9}{4} g_Y^2 - \frac{17}{24} g_1^2 - \frac{9}{8} g_2^2 - 4 g_s^2\right) p \quad , \quad \delta Z_{\nu} = \left(3 g_Y^2 - \frac{3}{4} g_1^2 - \frac{9}{4} g_2^2 + 6 \lambda\right) p .$$

As in the appendix B.1 the final result is presented without linear mass terms, poles and ι_ϵ-terms, which would cancel in the sum. The following contributions form the complete standard model effective potential to the order g^4, λ^2:

$$V_3 = \frac{\varphi^2}{2} \left[-\nu + \frac{1}{\beta^2} \left(\frac{1}{2} \lambda + \frac{3}{16} g_2^2 + \frac{1}{16} g_1^2 + \frac{1}{4} g_Y^2\right)\right] + \frac{\lambda}{4} \varphi^4 \tag{B.21}$$

$$- \frac{1}{12 \pi \beta} \left[{m_1}^3 + 3 {m_2}^3 + 4 {m_W}^3 + 2 {m_{WL}}^3 + 2 {m_Z}^3 + {m_{ZL}}^3 + {m_{\gamma L}}^3\right]$$

$$V_a = \frac{g_2^2}{32 \pi^2 \beta^2} \left[m_W^2 \left(2 - \frac{1}{c^2} + \frac{1}{2 c^4}\right) \left(\ln \frac{\beta}{3} - \frac{1}{12} \ln \bar{\mu}^2 \beta^2 - \frac{1}{6} c_1 + \frac{1}{4} c_2 + \frac{1}{4}\right)\right. \tag{B.22}$$

$$+\frac{1}{4}\left(1+\frac{1}{2c^2}\right)\left\{\left(m_1^2+3m_2^2\right)\left(-4\ln\frac{\beta}{3}+\ln\bar{\mu}^2\beta^2-c_2\right)+2m_2\left(m_1+m_2\right)\right\}$$

$$-4s^2m_2^2\ln\left(2m_2\right)-\frac{1}{2m_W}\left(1+\frac{1}{2c}\right)(m_1-m_2)^2(m_1+m_2)+2m_2m_Zs^2$$

$$-\frac{m_W}{2}\left(1+\frac{1}{2c^3}\right)(m_1+3m_2)-\frac{3}{4m_W^2}\left(m_1^2-m_2^2\right)^2\ln(m_1+m_2)$$

$$+\frac{1}{2m_W^2}\left\{m_W^4-2\left(m_1^2+m_2^2\right)m_W^2+\left(m_1^2-m_2^2\right)^2\right\}\ln\left(m_1+m_2+m_W\right)$$

$$+\frac{1}{4m_W^2}\left\{m_Z^4-2\left(m_1^2+m_2^2\right)m_Z^2+\left(m_1^2-m_2^2\right)^2\right\}\ln\left(m_1+m_2+m_Z\right)$$

$$+\left(\frac{1}{4c^2}-s^2\right)\left(m_Z^2-4m_2^2\right)\ln(2m_2+m_Z)+\frac{1}{2}\left(m_W^2-4m_2^2\right)\ln(2m_2+m_W)\Bigg]$$

$$V_b=\frac{g_2^2}{64\pi^2\beta^2}\Bigg[\left\{\left(c^4+\frac{1}{c^4}+4c^2+\frac{4}{c^2}-10\right)m_W^2+2\left(c^2-\frac{1}{c^2}\right)s^2m_2^2+\frac{s^4m_2^4}{m_W^2}\right\} \tag{B.23}$$

$$\times\ln(m_W+m_Z+m_2)+\left\{\left(5-4c^2\right)m_W^2-\frac{1}{m_W^2}\left(m_W^2c^2+m_2^2s^2\right)^2\right\}\ln(m_W+m_2)$$

$$-\frac{s^4}{m_W^2}\left(m_Z^2-m_2^2\right)^2\ln(m_Z+m_2)+m_W\left\{m_2\left(\frac{1}{c^2}-c^2+\frac{s^4}{c}\right)+m_1\left(1+\frac{1}{2c^3}\right)\right\}$$

$$+m_W^2\left\{\left(\frac{5}{2c^2}+\frac{5}{8c^4}-\frac{5}{4}\right)\left(2\ln\frac{\beta}{9\bar{\mu}}+c_2\right)+\frac{c^2}{2}-\frac{5}{2}+\frac{2}{c^2}+\frac{s^2}{c}\left(c^2-\frac{1}{c^2}\right)\right\}$$

$$-\frac{1}{2m_W^2}\left\{2\left(m_W^2-m_1^2\right)^2\ln(m_W+m_1)+\left(m_Z^2-m_1^2\right)^2\ln(m_Z+m_1)\right\}$$

$$+\left(4m_W^2-2m_1^2+\frac{m_1^4}{2m_W^2}\right)\ln(2m_W+m_1)+\frac{1}{c^2}\left(2m_Z^2-m_1^2+\frac{m_1^4}{4m_Z^2}\right)\ln(2m_Z+m_1)$$

$$+s^2m_2^2\left(2\ln m_2+\frac{s^2}{c}\right)+\frac{m_1^2}{2}\left(1+\frac{1}{2c^2}\right)+\frac{1}{m_W^2}\left(s^4m_2^4\ln m_2+\frac{3}{4}m_1^4\ln m_1\right)$$

$$+\frac{\varphi^2}{4g_2^2}\Big\{(g_2\tilde{c}+g_1\tilde{s})^4\ln(2m_{ZL}+m_1)+(g_2\tilde{s}-g_1\tilde{c})^4\ln(2m_{\gamma L}+m_1)$$

$$+2g_2^4\ln(2m_{WL}+m_1)+2(g_2\tilde{c}+g_1\tilde{s})^2(g_2\tilde{s}-g_1\tilde{c})^2\ln(m_{ZL}+m_{\gamma L}+m_1)$$

$$+4g_2^2g_1^2\left(\tilde{s}^2\ln(m_{WL}+m_{ZL}+m_2)+\tilde{c}^2\ln(m_{WL}+m_{\gamma L}+m_2)\right)\Big\}\Bigg]$$

$$V_i=\frac{1}{8\pi^2\beta^2}\Bigg[\left\{\frac{g_2^2m_f^2}{96}\left(10+\frac{17}{c^2}\right)+\frac{g_2^2n_fm_W^2}{36}\left(\frac{10}{c^2}-\frac{5}{c^4}-14\right)+g_s^2m_f^2\right\} \tag{B.24}$$

$$\times(\ln\bar{\mu}^2\beta^2-c_1+\frac{1}{2}+\frac{10}{3}\ln 2)-\frac{4g_2^2n_fm_W^2}{27}\left(\frac{10}{c^2}-\frac{5}{c^4}-14\right)\ln 2\Bigg]$$

$$V_j=\frac{g_Y^2}{128\pi^2\beta^2}\left[\left(9m_f^2-m_1^2-3m_2^2\right)\left(\ln\bar{\mu}^2\beta^2-c_1+\frac{3}{2}-\ln 4\right)+48m_f^2\ln 2\right] \tag{B.25}$$

$$V_m=\frac{g_2^2}{16\pi^2\beta^2}\Bigg[m_W^2\Bigg(\Big(-\frac{1}{4c^4}-\frac{1}{c^2}+\frac{5}{2}-c^2-\frac{c^4}{4}\Big)\ln(m_W+m_Z) \tag{B.26}$$

$$+\left(\frac{1}{8c^4}+\frac{1}{c^2}-5-4c^2\right)\ln(2m_W+m_Z)+\frac{31}{8}\ln\bar{\mu}^2\beta^2-\frac{11}{16}c_1-\frac{51}{16}c_2-\frac{251}{96}$$

$$-\frac{11}{12}c-\frac{5}{4c}+\frac{1}{8c^2}-4s^2\ln 2+\frac{1}{4}c^2(c-\frac{1}{2})+\frac{1}{8}\left(2-\frac{1}{c^4}\right)\ln c-\frac{51}{4}\ln\frac{\beta}{3}$$

$$+\left(\frac{1}{8c^4}-\frac{23}{4}+5c^2+\frac{1}{4}c^4\right)\ln m_W\Bigg)-m_Wm_{WL}(1+c)-2s^2m_{WL}^2\ln(2m_{WL})$$

$$+\left(\frac{1}{2}m_W^2-2c^2m_{WL}^2\right)\ln(2m_{WL}+m_Z)+\frac{1}{2}m_{WL}^2-\frac{m_{WL}^3}{m_W}$$

$$+\tilde{s}^2\Bigg\{\left(m_W^2-2m_{WL}^2-2m_{\gamma L}^2+\frac{\left(m_{WL}^2-m_{\gamma L}^2\right)^2}{m_W^2}\right)\ln(m_{WL}+m_{\gamma L}+m_W)$$

$$+m_{\gamma L}(m_{WL}-m_W)+\frac{m_{WL}^2m_{\gamma L}+m_{WL}m_{\gamma L}^2-m_{\gamma L}^3}{m_W}-\frac{\left(m_{WL}^2-m_{\gamma L}^2\right)^2\ln(m_{\gamma L}+m_{WL})}{m_W^2}\Bigg\}$$

$$+\tilde{c}^2\Big\{\qquad m_{\gamma L}\longrightarrow m_{ZL}\qquad\Big\}\Big]$$

$$V_p=-\frac{3\lambda^2\varphi^2}{32\pi^2\beta^2}\left[\ln\frac{9\bar{\mu}^2}{\beta^2}-c_2-2\ln\{m_1(m_1+2m_2)\}\right] \tag{B.27}$$

$$V_4=\frac{\varphi^2}{64\pi^2\beta^2}\left[\frac{g_2^4}{4}\left\{\left(\frac{1}{c^2}-\frac{1}{2c^4}-\frac{35}{4}\right)(\ln\bar{\mu}^2\beta^2-c_1)+\frac{293}{72}-\frac{1}{18c^2}-\frac{13}{18c^4}\right\}\right. \tag{B.28}$$

$$+\frac{g_2^4n_f}{27}\left(\frac{10}{c^2}-\frac{5}{c^4}-14\right)+g_Y^2\left(\frac{g_2^2s^2}{3c^2}-\frac{3g_Y^2}{4}+4g_s^2\right)\ln 4+g_2^2\left(\frac{g_Y^2}{2}+\lambda\right)\left(1+\frac{1}{2c^2}\right)$$

$$\left.+3g_Y^2\lambda\left(\ln\bar{\mu}^2\beta^2-c_1+\frac{3}{2}\right)\right]-\frac{1}{64\pi^2}\Big\{-4m_W^4-2m_Z^4-24m_f^4\ln 4$$

$$+\left(6m_W^4+3m_Z^4+m_1^4+3m_2^4-12m_f^4\right)\left(\ln\bar{\mu}^2\beta^2-c_1+\frac{3}{2}\right)\Big\}$$

$$V_z=\frac{1}{32\pi^2\beta^2}\left[\tfrac{1}{4}(m_1+3m_2)\Big\{g_2^2\left(2m_{WL}+4m_W+m_{ZL}\tilde{c}^2+2m_Zc^2\right)\right. \tag{B.29}$$

$$\left.+g_1^2\left(m_{ZL}\tilde{s}^2+2m_Zs^2\right)+m_{\gamma L}\left(g_2^2\tilde{s}^2+g_1^2\tilde{c}^2\right)\Big\}\right.$$

$$+\tfrac{1}{2}g_2g_1(m_1-m_2)\left\{2m_Zsc+(m_{ZL}-m_{\gamma L})\tilde{s}\tilde{c}\right\}+4g_2^2m_{WL}\left(m_W+m_Zc^2\right)$$

$$\left.+g_2^2m_W\left(4m_{\gamma L}\tilde{s}^2+\tfrac{8}{3}m_W+\tfrac{16}{3}m_Zc^2+4m_{ZL}\tilde{c}^2\right)+3\lambda\left(m_1m_2+\tfrac{1}{2}m_1^2+\tfrac{5}{2}m_2^2\right)\right].$$

B.3 SU(2)-Higgs model

In this section, for completeness, the potential of the SU(2)-Higgs model to order g^4, λ^2 is presented. It is readily obtained from the standard model results of section B.2 by performing the limit $g_1, g_Y \to 0$ and setting the number of families n_f to zero. With the masses

$$\begin{aligned} m_2^2 &= \lambda\varphi^2 - \nu + \frac{1}{12\beta^2}\left(6\lambda + \frac{9}{4}g^2\right) \quad , \quad m_1^2 = m_2^2 + 2\lambda\varphi^2 \, , \\ m_L^2 &= \frac{1}{4}g^2\varphi^2 + \frac{5}{6}\frac{g^2}{\beta^2} \quad , \quad m^2 = \frac{1}{4}g^2\varphi^2 \, , \end{aligned} \tag{B.30}$$

the final result is given by the sum of the following contributions:

$$V_3 = \frac{\varphi^2}{2}\left[-\nu + \frac{1}{\beta^2}\left(\frac{1}{2}\lambda + \frac{3}{16}g^2\right)\right] + \frac{\lambda}{4}\varphi^4 - \frac{1}{12\pi\beta}\left[{m_1}^3 + 3\,{m_2}^3 + 6\,m^3 + 3\,{m_L}^3\right] \tag{B.31}$$

$$\begin{aligned} V_a = \frac{3g^2}{128\pi^2\beta^2}\Bigg[& 2m^2\left(\ln\frac{\beta}{3} - \frac{1}{12}\ln\bar{\mu}^2\beta^2 - \frac{1}{6}c_1 + \frac{1}{4}c_2 + \frac{1}{4}\right) + m_2\left(m_1 + m_2\right) \\ & + \frac{1}{2}\left(m_1^2 + 3m_2^2\right)\left(-4\ln\frac{\beta}{3} + \ln\bar{\mu}^2\beta^2 - c_2\right) - \frac{1}{m}(m_1 - m_2)^2(m_1 + m_2) - m(m_1 + 3m_2) \\ & - \frac{1}{m^2}\left(m_1^2 - m_2^2\right)^2\ln(m_1 + m_2) + \left(m^2 - 4m_2^2\right)\ln(2m_2 + m) \\ & + \frac{1}{m^2}\left\{m^4 - 2\left(m_1^2 + m_2^2\right)m^2 + \left(m_1^2 - m_2^2\right)^2\right\}\ln\left(m_1 + m_2 + m\right)\Bigg] \end{aligned} \tag{B.32}$$

$$\begin{aligned} V_b = \frac{3g^2}{64\pi^2\beta^2}\Bigg[& m^2\left(\frac{5}{4}\ln\frac{\beta}{9\bar{\mu}} + \frac{5}{8}c_2 + \ln(2m_L + m_1)\right) + \frac{m_1^4}{4m^2}\ln m_1 + \frac{1}{2}m_1 m \\ & - \frac{1}{2m^2}(m^2 - m_1^2)^2\ln(m + m_1) + \left(2m^2 - m_1^2 + \frac{m_1^4}{4m^2}\right)\ln(2m + m_1) + \frac{1}{4}m_1^2\Bigg] \end{aligned} \tag{B.33}$$

$$\begin{aligned} V_m = \frac{g^2}{16\pi^2\beta^2}\Bigg[& \frac{m^2}{8}\left(31\ln\bar{\mu}^2\beta^2 - 66\ln m + 39\ln 3 - \frac{11}{2}c_1 - \frac{51}{2}c_2 - \frac{145}{4} - 102\ln\beta\right) \\ & - 3m_L m + \frac{3}{2}m_L^2 + \left(\frac{3}{2}m^2 - 6m_L^2\right)\ln(2m_L + m)\Bigg] \end{aligned} \tag{B.34}$$

$$V_p = -\frac{3\lambda^2\varphi^2}{32\pi^2\beta^2}\left[\ln\frac{9\bar{\mu}^2}{\beta^2} - c_2 - 2\ln\{m_1(m_1+2m_2)\}\right] \tag{B.35}$$

$$V_4 = \frac{m^2}{64\pi^2\beta^2}\left[g^2\left\{\frac{79}{24} - \frac{33}{4}(\ln\bar{\mu}^2\beta^2 - c_1)\right\} + 6\lambda\right] \tag{B.36}$$

$$-\frac{1}{64\pi^2}\left\{\left(9m^4 + m_1^4 + 3m_2^4\right)\left(\ln\bar{\mu}^2\beta^2 - c_1 + \frac{3}{2}\right) - 6m^4\right\}$$

$$V_z = \frac{1}{32\pi^2\beta^2}\left[\frac{g^2}{4}(m_1+3m_2)(3m_L+6m) + g^2m(8m+12m_L)\right. \tag{B.37}$$

$$\left.+3\lambda(m_1m_2 + \frac{1}{2}m_1^2 + \frac{5}{2}m_2^2)\right]. \tag{B.38}$$

Appendix C

Formulae for renormalization at $T = 0$

C.1 Abelian Higgs model

The self-energy of the vector field (in Minkowski space) has the structure

$$i\Pi^{\mu\nu}(q^2) = i\left(\Pi(q^2)g^{\mu\nu} + \Pi_L q^\mu q^\nu\right) . \tag{C.1}$$

Here the momentum independent part of $\Pi(q^2)$ is just the correction to the mass, and $\Pi_L(q^2)$ is irrelevant in Landau gauge because the propagator is transverse. The complete one-loop result without one-particle reducible tadpoles reads

$$\begin{aligned}\Pi(q^2) &= ie^2 A(m_\varphi^2) + \frac{ie^2}{3-2\epsilon}\Bigg\{\left(\frac{m^2-m_\varphi^2}{q^2}-1\right)A(m_\varphi^2) + \left(\frac{m_\varphi^2-m^2}{q^2}-1\right)A(m^2) \\ &\quad + \left[(1-\epsilon)8m^2 + \frac{(m_\varphi^2-m^2-q^2)^2}{q^2}\right]B(q^2,m_\varphi^2,m^2)\Bigg\} .\end{aligned} \tag{C.2}$$

Similarly, the one-loop self-energy of the Higgs particle is given by

$$\begin{aligned}\Pi_\varphi(q^2) &= 3i\lambda A(m_\varphi^2) + \left(3-2\epsilon-\frac{q^2}{m^2}\right)ie^2A(m^2) + \frac{ie^2}{2m^2}(m_\varphi^4-q^4)B(q^2,0,0) \\ &\quad + ie^2\left[(3-2\epsilon)2m^2 - 2q^2 + \frac{q^4}{2m^2}\right]B(q^2,m^2,m^2) + 18i\lambda^2v^2B(q^2,m_\varphi^2,m_\varphi^2) .\end{aligned} \tag{C.3}$$

Here $A(q^2)$ and $B(q^2,m_0^2,m_1^2)$ are the usual one- and two-point functions, defined in appendix A.2.

C.2 Standard model

The Landau gauge self-energy of the Higgs particle is given by

$$\Pi_\varphi(q^2) = 3i\lambda A(M_H^2) + i\lambda^2 v^2 \left[18B(q^2, M_H^2, M_H^2) + 6B(q^2, 0, 0)\right] \tag{C.4}$$

$$+\frac{ig_2^4 v^2}{8}\left[2\left\{\frac{1}{2M_W^2}A(M_W^2) + \left(3 - 2\epsilon - \frac{q^2}{M_W^2} + \frac{q^4}{4M_W^4}\right)B(q^2, M_W^2, M_W^2)\right.\right.$$

$$\left.\left. + \left(-\frac{1}{2} + \frac{q^2}{M_W^2} - \frac{q^4}{2M_W^4}\right)B(q^2, M_W^2, 0) + \frac{q^4}{4M_W^4}B(q^2, 0, 0)\right\} + \frac{1}{c^4}\left\{ M_W \to M_Z \right\}\right]$$

$$-\frac{ig_2^2}{4}\left[2\left\{\left(-2 + 2\epsilon + \frac{q^2}{M_W^2}\right)A(M_W^2) - \frac{(q^2 - M_W^2)^2}{M_W^2}B(q^2, M_W^2, 0) + \frac{q^4}{M_W^2}B(q^2, 0, 0)\right\}\right.$$

$$\left. + \frac{1}{c^2}\left\{ M_W \to M_Z \right\}\right] - 3ig_Y^2\left[2A(m_t^2) + (4m_t^2 - q^2)B(q^2, m_t^2, m_t^2)\right] .$$

Here M_W , M_Z and m_t are the zero temperature masses of the vector bosons and the top quark and c is the cosine of the Weinberg angle.

The fermion self energy can be written in the form

$$\Sigma^f(q) = \Sigma_S^f(q^2) + \Sigma_V^f(q^2)\not{q} + \Sigma_A^f(q^2)\not{q}\,\gamma_5 . \tag{C.5}$$

The γ_5-contribution is irrelevant for the mass counterterm $\delta m_t = \Sigma_S^f(m_t^2) + m_t\Sigma_V^f(m_t^2)$, which is obtained from

$$\Sigma_S^f(m_t^2) = -\frac{ig_Y^2 m_t}{2}[B(m_t^2, m_t^2, M_H^2) - B(m_t^2, m_t^2, 0)] - \frac{4}{3}g_s^2 I_S(0, m_t^2) \tag{C.6}$$

$$-\frac{g_2^2}{9}\left[4s^2 I_S(0, m_t^2) - \frac{s^2}{c}\left(3c - \frac{s^2}{c}\right)I_S(M_Z^2, m_t^2)\right] ,$$

$$\Sigma_V^f(m_t^2) = \frac{ig_Y^2}{4m_t^2}\left[2A(m_t^2) - A(M_H^2) + (M_H^2 - 2m_t^2)B(m_t^2, m_t^2, M_H^2) - 2m_t^2 B(m_t^2, m_t^2, 0)\right.$$

$$\left. - m_t^2 B(m_t^2, 0, 0)\right] - \frac{4}{3}g_s^2 I_V(0, m_t^2) \tag{C.7}$$

$$-g_2^2\left[\frac{1}{4}I_V(M_W^2, 0) + \frac{4}{9}s^2 I_V(0, m_t^2) + \left\{\frac{2s^4}{9c^2} + \frac{1}{72}\left(3c - \frac{s^2}{c}\right)^2\right\}I_V(M_Z^2, m_t^2)\right] .$$

Here the following short forms for typical self-energy contributions have been used:

$$I_S(m_0^2, m_1^2) = -im_1(3-2\epsilon)B(m_t^2, m_0^2, m_1^2) \tag{C.8}$$

$$\begin{aligned} I_V(m_0^2, m_1^2) = \frac{i}{2m_t^2 m_0^2}\Bigg[& \left\{(2-2\epsilon)m_0^2 + m_1^2 - m_t^2\right\} A(m_0^2) - (2-2\epsilon)m_0^2 A(m_1^2) \\ & + \Bigg\{ 2m_t^2 m_0^2(1-2\epsilon) + (3-2\epsilon)m_0^2\left(m_1^2 - m_0^2 - m_t^2\right) \\ & + \left(m_1^2 - m_0^2 - m_t^2\right)^2 \Bigg\} B(m_t^2, m_0^2, m_1^2) - \left(m_1^2 - m_t^2\right)^2 B(m_t^2, 0, m_1^2)\Bigg]. \end{aligned} \tag{C.9}$$

Bibliography

[1] E.W. Kolb and M.S. Turner, *The Early Universe* (Addison-Wesley, 1990)

[2] A.D. Sakharov, JETP Lett. 5 (1967) 24

[3] D. A. Kirzhnits and A. D. Linde, Phys. Lett. B42 (1972) 471

[4] V. A. Kuzmin, V. A. Rubakov and M. E. Shaposhnikov, Phys. Lett. B155 (1985) 36

[5] M. Joyce, T. Prokopec and N. Turok, preprint PUPT-1495;
M. Gleiser, talk at the *International Workshop on the Birth of the Universe and Fundamental Physics* (Rome, 1994);
M. Dine, Nucl. Phys. B, Proc. Suppl. 37A (1994) 127;
A. G. Cohen, D. B. Kaplan and A. E. Nelson, Annu. Rev. Nucl. Part. Sci. 43 (1993) 27

[6] A. Jakovác and A. Patkós, Z. Phys. C60 (1993) 361;
A. Jakovác, K. Kajantie and A. Patkós, Phys. Rev. D49 (1994) 6810

[7] K. Farakos, K. Kajantie, K. Rummukainen and M. Shaposhnikov, Nucl. Phys. B425 (1994) 67

[8] M. Gleiser and E. W. Kolb, Phys. Rev. D48 (1993) 1560;
P. Arnold and L. G. Yaffe, Phys. Rev. D49 (1994) 3003;
W. Buchmüller and Z. Fodor, Phys. Lett. B331 (1994) 124

[9] M. Reuter and C. Wetterich, Nucl. Phys. B408 (1993) 91 and B427 (1994) 291

[10] B. Bunk, E.-M. Ilgenfritz, J. Kripfganz and A. Schiller, Nucl. Phys. B403 (1993) 453;
K. Kajantie, K. Rummukainen and M. Shaposhnikov, Nucl. Phys. B407 (1993) 356

[11] Z. Fodor, J. Hein, K. Jansen, A. Jaster, I. Montvay and F. Csikor, Phys. Lett. B334 (1994) 405

[12] Z. Fodor, J. Hein, K. Jansen, A. Jaster and I.Montvay, Nucl. Phys. B439 (1995) 147

[13] P. Arnold, Phys. Rev. D46 (1992) 2628

[14] W. Buchmüller, T. Helbig and D. Walliser, Nucl. Phys. B407 (1993) 387

[15] M. E. Carrington, Phys. Rev. D45 (1992) 2933

[16] W. Buchmüller, Z. Fodor, T. Helbig and D. Walliser, Ann. Phys. 234 (1994) 260

[17] P. Arnold and O. Espinosa, Phys. Rev. D47 (1993) 3546, erratum ibid. D50 (1994) 6662

[18] J. E. Bagnasco and M. Dine, Phys. Lett. B303 (1993) 308

[19] A. Hebecker, Z. Phys. C60 (1993) 271

[20] Z. Fodor and A. Hebecker, Nucl. Phys. B432 (1994) 127

[21] W. Buchmüller, Z. Fodor and A. Hebecker, Phys. Lett. B331 (1994) 131

[22] W. Buchmüller, Z. Fodor and A. Hebecker, preprint DESY 95-028 (1995)

[23] J.I. Kapusta, *Finite-temperature field theory* (Cambridge Univ. Press, 1989)

[24] R. Jackiw, Phys. Rev. D9 (1974) 1686

[25] J.S. Langer, Physica A73 (1974) 61

[26] G. Slade, Commun. Math. Phys. 104 (1986) 573

[27] U.A. Wiedemann, Nucl. Phys. B406 (1993) 808

[28] D. Bödeker, W. Buchmüller, Z. Fodor and T. Helbig, Nucl. Phys. B423 (1994) 171

[29] E.J. Weinberg and A. Wu, Phys. Rev. D36 (1987) 2474

[30] T. Helbig, Ph.D. Thesis, Hamburg University (1993)

[31] C.G. Boyd, D.E. Brahm and S.D.H. Hsu, Phys. Rev. D48 (1993) 4963

[32] S. Weinberg, Phys. Rev. D9 (1974) 3357;
D. A. Kirzhnits and A. D. Linde, JETP 40 (1974) 628

[33] R.J. Rivers, *Path integral methods in quantum field theory* (Cambridge Univ. Press, 1987)

[34] R.R. Parwani, Phys. Rev. D45 (1992) 4695

[35] D. A. Kirzhnits and A. D. Linde, Ann. Phys. 101 (1976) 195

[36] A. D. Linde, Rep. Prog. Phys. 42 (1979) 389

[37] M. Laine, Phys. Lett. B335 (1994) 173

[38] M. Dine, R.G. Leigh, P. Huet, A. Linde and D. Linde, Phys. Rev. D46 (1992) 550

[39] J.R. Espinosa, M. Quirós and F. Zwirner, Phys. Lett. B314 (1993) 206

[40] G. Amelino-Camelia, Phys. Rev. D49 (1994) 2740

[41] S. Coleman, Phys. Rev. D15 (1977) 2929

[42] L. Dolan and R. Jackiw, Phys. Rev. D9 (1974) 3320

[43] M. Böhm, H. Spiesberger and W. Hollik, Fortschr. Phys. 34 (1986) 687

[44] Particle Data Group, K. Hikasa *et al.*, Phys. Rev. D45 (1992) S1

[45] A. Sirlin, Phys. Rev. D22 (1980) 971

[46] G. Degrassi and A. Sirlin, Nucl. Phys. B383 (1992) 73

[47] W. F. L. Hollik, Fortschr. Phys. 38 (1990) 165

[48] F. Jegerlehner, in *Testing the Standard Model—Proceedings of the 1990 Theoretical Advanced Study Institute in Elementary Particle Physics*, ed. by M. Cvetič and P. Langacker (World Scientific, Singapore, 1991) p. 476

[49] W.J. Marciano and A. Sirlin, Phys. Rev. D22 (1980) 2695

[50] W. Buchmüller and O. Philipsen, preprint DESY 94-202, to appear in Nucl. Phys. B

[51] M. Lüscher, unpublished notes (1988)

[52] J.M. Cornwall, R. Jackiw and E. Tomboulis, Phys. Rev. D10 (1974) 2428

[53] I.D. Lawrie, Nucl. Phys. B301 (1988) 685

[54] M. Laine, Phys. Rev. D51 (1995) 4525

[55] J. Zinn-Justin, *Quantum Field Theory and Critical Phenomena* (Clarendon Press, Oxford, 1993) pp. 242–243

[56] ibid., pp. 844–845

[57] H.B. Callan, *Thermodynamics* (Wiley, New York, 1960)

[58] P. Arnold and C. Zhai, Phys. Rev. D50 (1994) 7603